



PAPER • OPEN ACCESS

Competing role of interactions in synchronisation of exciton–polariton condensates

To cite this article: Saeed A Khan and Hakan E Türeci 2017 *New J. Phys.* **19** 105008

View the [article online](#) for updates and enhancements.

Related content

- [A polariton graph simulator](#)
Pavlos G Lagoudakis and Natalia G Berloff
- [Stochastic spin flips in polariton condensates: nonlinear tuning from GHz to sub-Hz](#)
Yago del Valle-Inclan Redondo, Hamid Ohadi, Yuri G Rubo et al.
- [Topical Review](#)
J Keeling, F M Marchetti, M H Szymaska et al.



PAPER

Competing role of interactions in synchronisation of exciton–polariton condensates

OPEN ACCESS

RECEIVED

29 April 2017

REVISED

26 July 2017

ACCEPTED FOR PUBLICATION

1 September 2017

PUBLISHED

31 October 2017

Saeed A Khan and Hakan E Türeci

Department of Electrical Engineering, Princeton University, Princeton, NJ 08544, United States of America

E-mail: saeedk@princeton.edu**Keywords:** synchronisation, non-Hermitian modal theory, nonlinear dynamicsSupplementary material for this article is available [online](#)

Original content from this work may be used under the terms of the [Creative Commons Attribution 3.0 licence](#).

Any further distribution of this work must maintain attribution to the author(s) and the title of the work, journal citation and DOI.

**Abstract**

We present a theoretical study of synchronisation dynamics of incoherently pumped exciton–polariton condensates in coupled polariton traps. Our analysis is based on a coupled-mode theory for the generalised Gross–Pitaevskii equation, which employs an expansion in non-Hermitian, pump-dependent modes appropriate for the pumped geometry. We find that polariton–polariton and reservoir–polariton interactions play competing roles and lead to qualitatively different synchronised phases of the coupled polariton modes as pumping power is increased. Crucially, these interactions can also act against each other to hinder synchronisation. We map out a phase diagram and discuss the general characteristics of these phases using a generalised Adler equation.

Synchronisation is a ubiquitous phenomenon in dynamical oscillating systems [1] that has recently seen renewed interest across diverse setups, from electro/opto-mechanical oscillators [2–5], to lasers [6–8], trapped atoms [9–11], and many-oscillator arrays [12–14]. Recently quantum effects have also been explored [15–19]. In this work, we focus on the manifestation of synchronisation in incoherently pumped exciton–polariton systems, where this phenomenon appears as the natural mechanism to explain [20] the formation of spatially extended condensates across disorder-generated localised photonic traps, prevalent in early experiments [21]. It was later pointed out [22] that synchronisation can also take place between extended modes that overlap. While such effects are present in photon lasers as well [23–25], what distinguishes polariton condensates are strong nonlinear interactions [26, 27]. One may then ask whether these interactions can give rise to *qualitatively* different synchronisation physics in polariton condensates. Our present work aims to answer this question.

Fundamentally, we study the synchronisation of two coupled ‘oscillators’; however, the unique platform of exciton–polariton condensates under incoherent pumping modifies this picture significantly. In these systems, an uncondensed fraction of polaritons (the ‘reservoir’) is deposited by the pump, typically at high energies; interactions amongst them give rise to stimulated scattering towards lower energy states, which can lead to condensation at a threshold pump strength P_1^L . The condensate mode above this threshold power appears with a self-organised frequency and associated spatial pattern. Typically, above a second threshold P_2^L a second mode condenses with generally a different oscillation frequency [28, 29]. While this threshold physics is similar to the photon laser, exciton–polaritons distinguish themselves with strong, pump-dependent nonlinear interactions, which come in two varieties. Quasi-particles belonging to the condensate interact, giving rise to purely energetic effects. On the other hand, the deposited reservoir polaritons provide both a repulsive potential and the source of gain that allows condensation in the first place. Crucially, these interactions strongly depend on quasi-particle density, and hence pump power, leading to an effective *pump-dependent* coupling between the oscillators that is different from Huygens’ original clock oscillator model of synchronisation [30, 31]. The interactions mediate frequency modulation, which we find plays a crucial role in eventually locking the two oscillators to a single frequency at the synchronisation threshold. In fact, over the same pumping range, synchronisation is no longer observed if interactions are turned off. Strong interactions thus enable the synchronisation threshold to be reached even for far detuned modes at low powers; this is different from the laser, where relatively weaker interactions fail to lower the threshold for synchronisation below that of other instabilities (e.g. a third mode

turning on), except under carefully constructed situations that maximise modal coupling and minimise detuning [32].

This simple emergence of frequency synchronisation beyond a threshold power is not the full story, however; the different nature and origin of the two distinct nonlinear interactions, a feature quite unique to polariton condensates, reveals even richer dynamics. When one interaction is dominant relative to the other, synchronisation is indeed aided by frequency modulation mediated by that interaction. Crucially, the properties of the emergent synchronised state depend strongly on the nature of this dominant interaction. However, we find that when these strong interactions have comparable strengths—in a quantifiable way that we derive—the situation changes completely: the interactions play competing roles that actually prevent a synchronised state from being reached.

To efficiently capture the nonlinear, pump-dependent interactions and reservoir dynamics present in this system, we employ a temporal coupled mode theory (TCMT) of condensate dynamics introduced in our recent work [33]. This approach is built upon the standard description of polariton condensation via the generalised Gross–Pitaevskii equation (gGPE), but provides a more economical framework for both numerical and analytical studies. In particular, the modal theory enables us to develop an analytical model for the role of interactions based on a multivariable generalised Adler equation, and to numerically study the long-time limit of dynamics for a wide parameter regime. Our key result is a phase diagram which maps out the presence of distinct synchronised phases when either of the two interactions is dominant, and a desynchronised phase when both interactions are actively competing.

The rest of this paper is organised as follows: in section 1, we briefly review the non-Hermitian coupled-mode theory that is the foundation for the analysis to follow. In section 2, we introduce the model system for our study of synchronisation: two coupled, detuned polariton traps under uniform incoherent pumping. The coupled-mode theory is specialised to this case, and an amplitude-phase-intensity basis is introduced to express the modal equations more efficiently. A generalised Adler equation for the phase dynamics is analysed in section 3, which provides intuitive insight into the role played by interactions in the existence of a synchronised phase. Finally, in section 4, the emergence of stable synchronised fixed points as a function of pump power is investigated, and a phase diagram is mapped out. Analytical results are compared both with full numerical simulations of the TCMT, as well as select simulations of the gGPE using a split-step integrator; excellent agreement is found amongst the various methods.

1. Review of non-Hermitian coupled mode theory

1.1. Generalised Gross–Pitaevskii equation (gGPE)

The dynamics of exciton–polariton condensation under incoherent pumping has been very effectively described via a gGPE. This takes the form of a complex dynamical equation for the order parameter $\Psi(\mathbf{r}, t)$, coupled to a rate equation for the incoherent reservoir population n_R deposited by the pump (we set $\hbar = 1$) [34]:

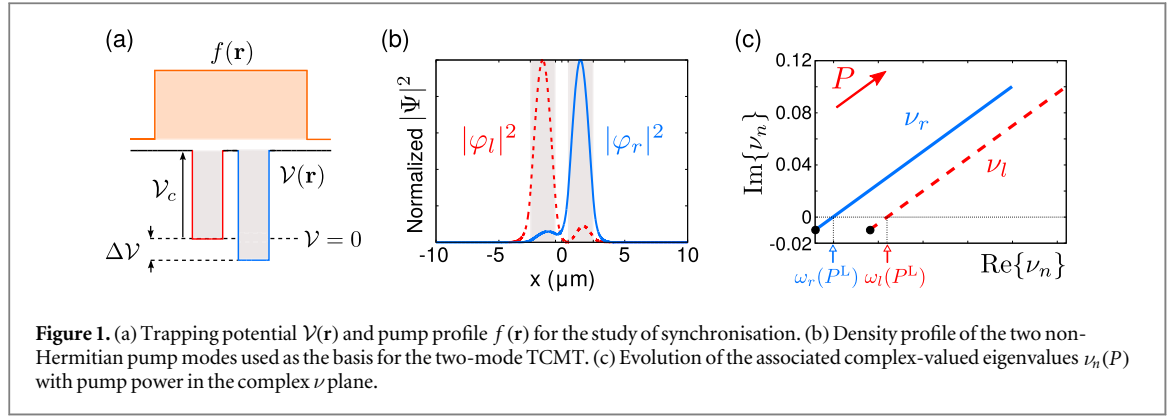
$$i\partial_t\Psi = \left[-\frac{\nabla^2}{2m} + \mathcal{V}(\mathbf{r}) + \left(g_R + i\frac{R}{2} \right) n_R + g|\Psi|^2 - i\frac{\gamma_c}{2} \right] \Psi, \quad (1a)$$

$$\partial_t n_R = Pf(\mathbf{r}) - \gamma_R n_R - R n_R |\Psi|^2. \quad (1b)$$

Here, $\mathcal{V}(\mathbf{r})$ is an arbitrary confining potential; for our study of synchronisation, $\mathcal{V}(\mathbf{r})$ describes two tunnel-coupled and detuned polariton traps. Such models are relevant to condensation in disordered semiconductor microcavities, as well as recently realised coupled micropillar systems [35, 36]. The pump depositing the exciton reservoir has strength P and spatial profile $f(\mathbf{r})$. We consider condensation under uniform incoherent pumping; the confining and pumping geometries are depicted in figure 1(a).

Scattering from the exciton reservoir provides gain (rate R) leading to the formation of a coherent condensate when polariton losses γ_c are overcome. The reservoir relaxation rate γ_R encapsulates all loss processes other than scattering into the condensate. Most important for the purpose of this work are the two distinct types of interparticle interactions present: between polaritons within the condensate (strength g), and between reservoir excitons and condensate polaritons (strength g_R). Within the mean-field description employed here, interactions provide repulsive potentials that lead to polaritons experiencing pump-dependent frequency blueshifts. Note that reservoir-mediated gain and blueshift arise from separate physical processes (scattering and repulsive interactions respectively), and are thus characterised by generally different parameters R and g_R . Finally, an additional diffusion term for reservoir excitons may be included in equation (1b); however, this term is often neglected, owing to the much heavier mass of reservoir excitons relative to that of condensate polaritons. We justify this approximation in appendix G.

Unfortunately, the set of coupled nonlinear partial differential equations described by equations (1a) are numerically expensive to solve and provide limited analytic insight except in some special cases [37]. However,



from this starting point we are able to arrive at a modal description that proves much more efficient. This approach, originally developed in [33], projects equations (1a) and (1b) onto a spatial basis consisting of pump-dependent non-Hermitian modes, which we introduce next. The result of this projection is a set of ordinary differential equations for time-dependent basis expansion coefficients; these equations, expressed in equations (7a) and (7b), comprise our temporal coupled-mode theory (TCMT).

1.2. Non-Hermitian pump modes

To define the spatial basis for the TCMT, we begin by considering a linearised version of the gGPE, in the absence of polariton–polariton interactions and pump depletion. We drop nonlinear terms $\propto |\Psi|^2$, and replace the reservoir density by its undepleted value, $n_R = Pf(\mathbf{r})/\gamma_R$; then equations (1a) and (1b) reduce to the single linearised dynamical equation:

$$i\partial_t\Psi = \left[-\frac{\nabla^2}{2m} + \mathcal{V}(\mathbf{r}) + \frac{1}{\gamma_R} \left(g_R + i\frac{R}{2} \right) Pf(\mathbf{r}) - i\frac{\gamma_c}{2} \right] \Psi \equiv \mathcal{H}_L(P)\Psi. \quad (2)$$

Equation (2) provides an exact description of the physical situation before and *just* up to the formation of a condensate, but is clearly not equivalent to the full gGPE beyond the condensation threshold, where $|\Psi|^2 \neq 0$. For our purposes, however, equation (2) is used to *define* the linear non-Hermitian generator $\mathcal{H}_L(P)$, which incorporates the trapping potential $\mathcal{V}(\mathbf{r})$ and the pump-induced potential. Then, the pump power P is arbitrarily tunable, and serves to parametrise the pump dependence of this linear generator. The computational modes $\{\varphi_n\}$ we employ for our modal theory are then eigenmodes of this generator, defined as:

$$\mathcal{H}_L(P)\varphi_n(\mathbf{r}; P) = \nu_n(P)\varphi_n(\mathbf{r}; P). \quad (3)$$

Since $\mathcal{H}_L(P)$ is non-Hermitian, its eigenmodes are not orthogonal relative to the standard inner product. However, it can be shown that by introducing a set of dual modes $\{\bar{\varphi}_n\}$ which satisfy the dual non-Hermitian eigenproblem $\mathcal{H}_L^*(P)\bar{\varphi}_n = \nu_n^*(P)\bar{\varphi}_n$, a complete basis may be obtained, satisfying the biorthogonality relation [38, 39]:

$$\int_{\mathcal{P}} d\mathbf{r} \bar{\varphi}_n^*(\mathbf{r}; P)\varphi_m(\mathbf{r}; P) = \delta_{nm}, \quad (4)$$

where \mathcal{P} is the minimal region beyond which the pump has vanishing strength. It is easy to see that $\bar{\varphi}_n^* = \varphi_n$, so that equation (4) reduces to a self-orthogonality relation:

$$\int_{\mathcal{P}} d\mathbf{r} \varphi_n(\mathbf{r}; P)\varphi_m(\mathbf{r}; P) = \delta_{nm}. \quad (5)$$

The linear dynamics described by equation (2) are encoded in the pump-dependent, complex eigenvalues $\nu_n(P) = \omega_n(P) + i\gamma_n(P)$ of each eigenmode. The real part $\omega_n(P)$ represents the modal frequency, determined by the confining potential $\mathcal{V}(\mathbf{r})$ and the blueshift due to reservoir excitons ($\propto g_R$). On the other hand, the imaginary parts $\gamma_n(P)$ of the eigenvalues characterise non-Hermitian pumping and dissipation: they describe the net gain experienced by the n th mode at a given pump power. For low enough pump powers, all modal eigenvalues have negative imaginary parts, indicative of a below-threshold regime—all modes experience net loss. As the pump power increases, the modal eigenvalues flow in the complex plane as the gain from the pump increases. For a specific pump strength $P = P_n^L$, which we refer to as the linear threshold power, the n th eigenmode acquires a vanishing imaginary part; for $P > P_n^L$, this mode experiences gain (see figure 1(c)). A threshold pump power can be associated with each mode; it is determined by how effective the specific mode is at utilising gain from the pump [33], in the presence of the confining and pump-induced potential. Modes that are spatially configured to utilise the pump more efficiently have lower threshold pump values.

Due to their explicit pump dependence and associated threshold physics, we refer to the non-Hermitian eigenmodes of the linear generator as *pump modes* from this point on. Furthermore, the linear threshold power value P_n^L associated with each pump mode $\{\varphi_n\}$ hints at a natural ordering principle for these non-Hermitian modes. This allows us to define a suitable truncation scheme for an expansion in a basis of these pump modes, which we discuss next.

1.3. Coupled-mode equations

Having defined our computational basis, we are now equipped to tackle the full nonlinear problem posed by equations (1a) and (1b). We proceed to expand the condensate order parameter $\Psi(\mathbf{r}, t)$ in the set of pump-dependent non-Hermitian pump modes with *time-dependent* coefficients:

$$\Psi(\mathbf{r}, t) = \sum_{n=1}^N a_n(t) \varphi_n(\mathbf{r}; P), \quad (6)$$

where the sum may extend over an arbitrary number N of pump modes. The choice of modes to include in this expansion may seem unclear. Note that a truncation scheme that retains only pump modes with the lowest frequencies would not be appropriate in all cases: the non-Hermitian dynamics can lead to condensation in a mode that is *not* the lowest frequency mode for a given pumping potential. Instead, a truncation based on the linear threshold powers of the pump modes is more appropriate. We choose a basis of size N to comprise of the modes with the N lowest linear threshold power values. In this way, the modes that best optimise gain from the pump are retained in the basis expansion [33].

With the expansion placed on firm footing, we may now project the fully nonlinear equations (1a) and (1b) onto this basis, and integrate out the spatial dependence using relation (5). We leave the details of this procedure for appendix A; the resulting dynamical equations corresponding to equations (1a) and (1b) respectively are given by:

$$i \frac{d}{dt} a_n = \nu_n(P) a_n + g \sum_{mkq} A_{nmkq} a_m a_k a_q^* + \left(g_R + i \frac{R}{2} \right) \sum_m N_{nm} a_m, \quad (7a)$$

$$\frac{d}{dt} N_{nm} = -\gamma_R N_{nm} - \sum_{kq} \left\{ \left[\frac{R}{\gamma_R} P B_{nmkq} + A_{nmkq} (i\nu_k - i\nu_q^*) \right] + \left(\frac{d}{dt} \right) \right\} a_k a_q^*. \quad (7b)$$

In the above, we have introduced dynamical variables describing the evolving reservoir density, referred to as the reservoir matrix elements $N_{nm}(t)$. These are given by:

$$N_{nm} = \int_{\mathcal{P}} d\mathbf{r} \varphi_n \left[n_R - \frac{P}{\gamma_R} f(\mathbf{r}) \right] \varphi_m^*, \quad (8)$$

and describe the change in reservoir density relative to its unsaturated value. Lastly, we define the spatial overlap matrix elements:

$$A_{nmkq} = \int_{\mathcal{P}} d\mathbf{r} \varphi_n \varphi_m \varphi_k \varphi_q^*, \quad B_{nmkq} = \int_{\mathcal{P}} d\mathbf{r} f(\mathbf{r}) \varphi_n \varphi_m \varphi_k \varphi_q^*. \quad (9)$$

Equations (7a) and (7b) constitute the TCMT with nonlinear interactions and pump depletion. In equation (7a), we clearly see the eigenvalues $\nu_n(P) = \omega_n(P) + i\gamma_n(P)$ controlling linear dynamics. All remaining terms incorporate the nonlinear effects neglected in the linear theory; the term $\propto g$ describes polariton–polariton interactions, with the mode overlap integrals A_{nmkq} describing self-interaction and cross-mode interaction contributions. The final term with reservoir matrix elements N_{nm} describes the effect of reservoir depletion; note that these reservoir matrix elements are themselves dynamically determined by equation (7b).

The TCMT provides an efficient spectral description of the nonlinear, non-Hermitian dynamics of polariton condensation, for arbitrary pumping and trapping potentials. In [33], TCMT simulations were compared with direct split-step integration of the gGPE, and the results found to agree very favourably in a variety of settings. In the next section, we employ this TCMT for an analytical and numerical study of synchronisation in coupled polariton traps.

2. Condensation in coupled polariton traps

2.1. System and parameters

For the study of synchronisation, we consider a confining potential $\mathcal{V}(\mathbf{r})$ that describes two coupled polariton traps, and a uniform incoherent pump across both traps (see figure 1(a)). Generally, there is a (low) pumping range wherein it is accurate to truncate the TCMT to only the two most preferred pump modes, namely the modes with lowest linear threshold powers. We consider specifically a detuned trap regime here, where these two

modes are predominantly confined to the left or right trap; hence we denote the modes by φ_l and φ_r respectively, as shown in figure 1(b). We emphasise again that these modes are *not* simply eigenmodes of the individual traps; rather they account for tunnelling between the traps, the unsaturated pump, and dissipation through cavity loss. Under pumping with a wide, homogeneous pump spot, it is the static trapping potential that predominantly determines the modes φ_l , φ_r ; the non-Hermitian pump-induced potential does not modify the modes directly in this case, but our analysis does not make any explicit simplifications using this fact. However the non-Hermitian potential does control the evolution of modal eigenvalues with pump power: the homogeneous pump spot ensures this evolution is similar for both eigenvalues (see figure 1(c)). Furthermore, both modes have an approximately equal linear threshold power P^L ; this is evident in how the eigenvalues cross the real line concurrently as pump power is increased. In the absence of pump-induced repulsion, the modal frequencies are ω_{l0} and ω_{r0} , determined by the trapping potential alone; we choose $\omega_{l0} > \omega_{r0}$, and define the bare pump mode detuning $\Delta\omega \equiv \omega_{l0} - \omega_{r0}$; for the potential landscape $\mathcal{V}(\mathbf{r})$ chosen here, $\Delta\omega_0 = 0.12$ meV, a typical value consistent with modal detunings in a variety of polariton trapping structures [21, 36]. For concreteness, we set $R = 0.1 \mu\text{m}^2$ meV, $m^{-1} = 0.59 \mu\text{m}^2$ meV, $\gamma_c = 1$ meV, and $\gamma_R = 10$ meV.

Note that we have chosen to operate in the regime of fast reservoir relaxation, $\gamma_R \gg \gamma_c$, which is relevant for condensation in disordered semiconductor quantum wells. More importantly, in the opposite case where $\gamma_R \ll \gamma_c$, we find a tendency towards strongly multimode behaviour, in agreement with recent numerical studies in this non-adiabatic regime [33, 40, 41]. The complicated dynamics can in fact be captured quite effectively by the TCMT, provided we include more than two modes in our basis (see appendix F). Therefore, to study dynamics within a two-mode approximation, we restrict ourselves to the fast reservoir relaxation regime.

2.2. Amplitude-phase-intensity basis

The condensate wavefunction in the two-mode TCMT is given by equation (6) for $n = l, r$, with the time-dependence entirely included in the mode coefficients $\{a_n(t)\}$. For the study of synchronisation, it proves useful to access the amplitude and phase dynamics directly; to this end we write the coefficients in a phasor representation, $a_n(t) = \bar{a}_n(t)e^{-i\phi_n(t)}$, $n = l, r$, and then cast equations (7a) and (7b) in terms of the dynamical variables $\{\phi, z, \rho\}$:

$$\phi = \phi_l - \phi_r, \quad z = \frac{\bar{a}_l^2 - \bar{a}_r^2}{\bar{a}_l^2 + \bar{a}_r^2}, \quad \rho = \bar{a}_l^2 + \bar{a}_r^2, \quad (10)$$

where ϕ is the relative phase, z the normalised modal intensity imbalance, and ρ the total intensity. Note that both $\phi \in [-\pi, \pi]$, and $z \in [-1, 1]$ are bounded variables, while ρ generally increases monotonically with the pump power P ; these observations prove very useful in our analysis later. Furthermore, in the regime of fast reservoir relaxation the reservoir matrix elements N_{nm} can be solved for in terms of the coefficients $\{a_n\}$, so that the $\{\phi, z, \rho\}$ variables are sufficient for a full description of the reservoir-condensate system.

A large body of earlier work on synchronisation [42] concerns itself with weakly coupled Hermitian systems: the total intensity ρ is a conserved quantity and oscillator amplitudes are deemed to be approximately stationary so that $\dot{z} \approx 0$, thereby allowing a phase-only description of the dynamics. In the desynchronized regime, the modes typically evolve at two distinct frequencies, namely the blueshifted trap frequencies, but modified by nonlinear interactions. The phases $\phi_{l,r}(t)$ then exhibit drift-like evolution. On the other hand, in the synchronised regime the two modes begin oscillating at the *same* unique frequency Ω_0 . When this occurs, both phases $\phi_{l,r}(t)$ exhibit a linear drift in time with the same drift constant (given by the synchronized frequency): $\Omega_0 t$, plus (in general) a constant offset. Crucially, then, it follows that the *relative* phase $\phi = \phi_l - \phi_r$ becomes *stationary* in time, $\dot{\phi} = 0$. This stationary relative phase serves an analytic signature of frequency synchronisation in such phase-only systems.

For the non-Hermitian, pump-dependent system under consideration here, we find it crucial to keep track of z and ρ dynamics in addition to the relative phase evolution. Oscillations in z and ρ are pump-dependent and may be large (see appendix C), so that the aforementioned approximations are not always valid. More importantly, while the relative phase may become stationary momentarily ($\dot{\phi} = 0$), we find that this state can only persist if $\dot{z} = \dot{\rho} = 0$ concurrently, and if the state is stable to fluctuations in *any* of these dynamical quantities. The requirement of such stable fixed points in $\{\phi, z, \rho\}$ space is then the analytic signature of synchronisation; comparisons between analytic and numerical results in section 4.2 confirm that the modal frequency detuning does in fact vanish at such fixed points.

Although the present system is not described by a phase-only model, the phase dynamics still remain quite informative: since $\dot{\phi} = 0$ is still a necessary (though not sufficient) condition for synchronisation to occur, it can place strong constraints on the synchronised phase, which we will explore next.

3. Generalised Adler equation

One of the earliest models of synchronisation involves the standard single-variable Adler equation [43]:

$$\dot{\phi} = \Omega - F \sin(\phi). \quad (11)$$

The Adler equation describes the dynamics of the relative phase ϕ , of two coupled oscillators for example, in the presence of a detuning term Ω that causes ϕ to drift linearly in time, and a coupling term $F \sin(\phi)$ that encourages its pinning to a constant value. Clearly, the synchronised $\dot{\phi} = 0$ solution is possible only if $-F < \Omega < F$, namely when the detuning term is small enough compared to the coupling. This model very successfully describes a broad range of synchronisation and phase locking dynamics, from injection locking of oscillators to an external drive [44, 45], to the synchronisation of coupled oscillators within a phase-only picture [46].

In the present case, a somewhat more complicated equation for the relative phase ϕ may also be obtained by transforming equations (7a) and (7b) to $\{\phi, z, \rho\}$ space as defined in equation (10); we refer to it as the generalised Adler equation:

$$\dot{\phi} = \Omega(z, \rho) - \rho F(\phi, z). \quad (12)$$

In analogy with the standard Adler equation, we refer to the ϕ -independent term $\Omega(z, \rho)$ as the detuning term (generally *not* just the same as the bare pump mode detuning $\Delta\omega_0$), and $\rho F(\phi, z)$ as the coupling term, which is periodic in ϕ . The ρ dependence of both terms reflects the pump-dependent nature of the nonlinear modal interaction. Note that Ω in equation (11) represents the bare frequency detuning of the *uncoupled* oscillators, and not the actual emergent detuning in the presence of coupling. Similarly, the detuning term $\Omega(z, \rho)$ is *not* the emergent detuning between the two coupled polariton modes; the latter is determined via simulation of the modal equations (see section 4.2).

The condition for $\dot{\phi} = 0$ imposed by the generalised Adler equation becomes:

$$\min_{\phi} \{\rho F(\phi, z)\} < \Omega(z, \rho) < \max_{\phi} \{\rho F(\phi, z)\}, \quad (13)$$

where $\max_{\phi} / \min_{\phi} \{f\}$ are the maximum/minimum values respectively taken by $f(\phi, z, \rho)$ as ϕ varies in $[-\pi, \pi]$, for a given (z, ρ) . Equation (13) implies that synchronisation is again possible only when the detuning is small enough compared to the coupling term; now, however, these terms are no longer constants like in equation (11), but are rather configuration dependent. To understand the implications of this constraint, we study the detuning and coupling terms separately, beginning with the former.

3.1. Nonlinear detuning modification

The detuning term $\Omega(z, \rho)$ includes the bare modal frequency difference and its modification due to nonlinear interactions. Here, we will see that this detuning term provides intuitive insight into the effect of nonlinear interactions on synchronisation dynamics. The full expression for the detuning term is given by equation (B.5) in appendix B; in the main text, we find it more instructive to present the form $\Omega(z, \rho)$ takes for specific regimes. In the absence of any repulsive interactions, $g, g_R = 0$, the detuning term is a constant equal to the bare pump mode detuning,

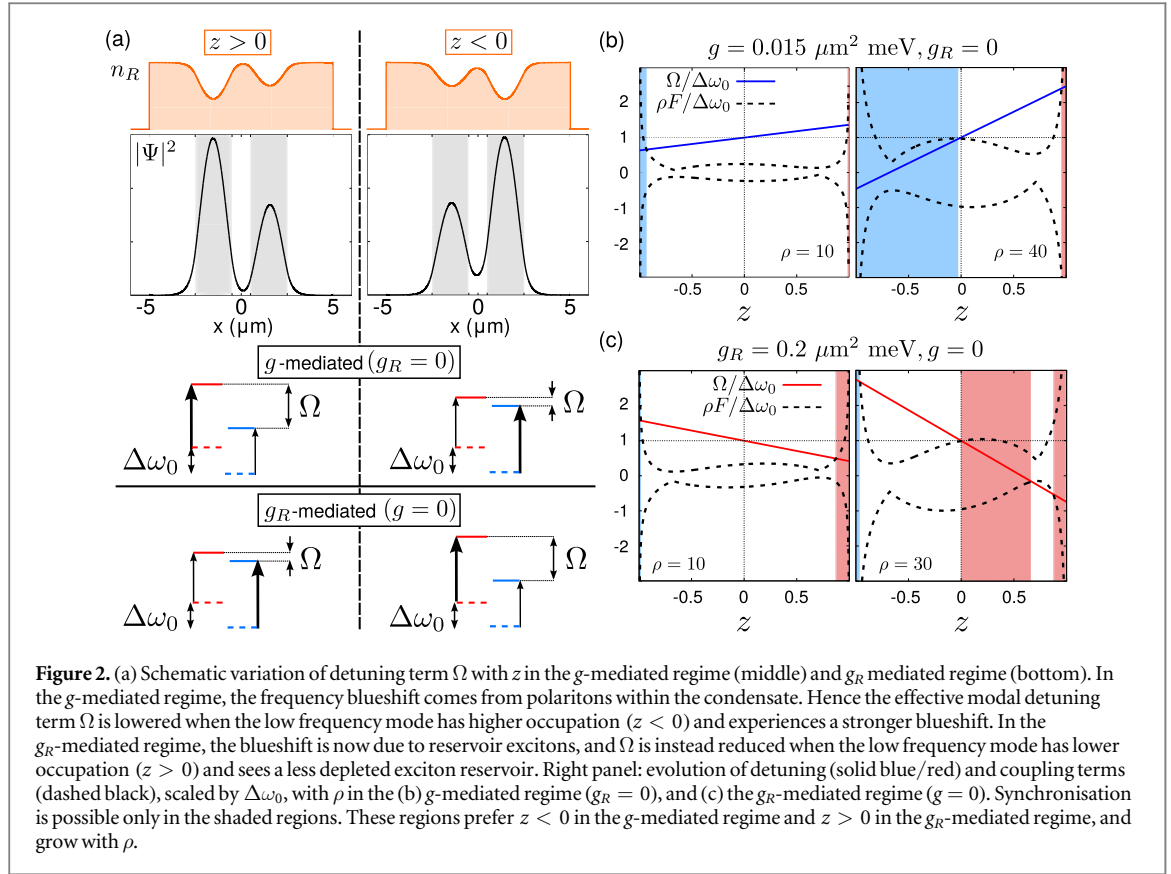
$$\Omega = \Delta\omega_0 \quad [g = g_R = 0] \quad (14)$$

independent of the pump power. The situation becomes more interesting once either type of repulsive interaction is active. If only interactions of polaritons within the condensate are considered—we define this as the g -mediated regime ($g_R = 0$)—the detuning term becomes:

$$\Omega = (\omega_{l0} + gA_{lll}\bar{a}_l^2 + 2gA_{llr}\bar{a}_r^2) - (\omega_{r0} + gA_{rrr}\bar{a}_r^2 + 2gA_{rrl}\bar{a}_l^2) \quad [g_R = 0]. \quad (15)$$

We have momentarily reverted to amplitude variables \bar{a}_n since each term is intuitively clearest here. The first bracketed term represents the blueshift of the the left trap mode due to repulsion from polaritons occupying that mode ($\propto A_{lll}\bar{a}_l^2$), and from polaritons occupying the right trap mode ($\propto A_{llr}\bar{a}_r^2$); the latter arises since the modes have nonzero spatial overlap. The second bracketed term is the corresponding blueshift of the right trap mode. Here $\frac{A_{llr}}{A_{lll}} \approx \frac{A_{rrl}}{A_{rrr}} \simeq 0.1$, so that the ‘direct’ blueshift is more important, and causes the mode with higher occupation to be more strongly blueshifted due to g . A reduction in the detuning term—which aids synchronisation, as per equation (13)—thus requires the low frequency mode (r) to experience a stronger blueshift, which is possible when this mode has higher occupation ($\bar{a}_r^2 > \bar{a}_l^2$), namely $z < 0$, as depicted in figure 2(a).

In the g_R -mediated regime where only interactions between reservoir excitons and condensate polaritons are active ($g = 0$), we have instead:



$$\Omega = \left(\omega_l(P) + g_R \frac{\rho \gamma_c}{\gamma_R} N_{ll}(z) \right) - \left(\omega_r(P) + g_R \frac{\rho \gamma_c}{\gamma_R} N_{rr}(z) \right) \quad [g = 0]. \quad (16)$$

The exciton repulsion $\propto g_R$ now linearly blueshifts the mode frequencies, lending them the P dependence shown in figure 1(c); the homogeneous pump spot ensures an equal blueshift that leaves the pump mode detuning unchanged, $\omega_l(P) - \omega_r(P) = \Delta\omega_0$. However, condensate formation depletes the exciton reservoir, since the latter serves as the source of gain. In particular, the higher the occupation of a mode, the more depleted is the exciton reservoir it sees. This reservoir depletion reduces the reservoir-mediated blueshift experienced by each mode; in the detuning term, this reduction is captured by the N_{nn} elements, which measure the reservoir depletion seen by mode n , and are explicitly negative (see equation (8)). To reduce the detuning term in this case, the low frequency mode (r) again needs to be more strongly blueshifted; however, due to the different blueshift mechanism, the lower frequency mode (r) must now have a *lower* occupation ($\bar{a}_r^2 < \bar{a}_l^2$), namely $z > 0$, since it then sees a less depleted exciton reservoir and can experience a stronger blueshift. This is exactly the opposite to the g -mediated case (see figure 2(a)). Hence, we see a configuration-dependence to the reduction of the detuning term in the generalised Adler equation, with the g - and g_R -mediated regimes preferring opposite configurations.

Finally, note the additional prefactor of $\gamma_c/\gamma_R = 0.1$ relative to the g -mediated case, which weakens the g_R mediated blueshift. This can be explained as follows: for larger values of γ_R , the pump threshold for condensation increases. The stronger pumping allows for a stronger scattering $\propto R|\Psi|^2$ from the reservoir to the condensate before reservoir depletion becomes important, which in turn means a higher condensate occupation is possible (for fixed polariton loss rate γ_c). The saturated reservoir density, however, is unchanged, since the stronger scattering uses up the additional pump power. Therefore, reservoir-dependent terms are reduced by a factor of γ_c/γ_R relative to terms that depend on the condensate density alone.

3.2. Pump-dependent coupling

Moving on to the coupling term $\rho F(\phi, z)$, our choice of variables immediately indicates its growth with pump power via the explicit scaling by ρ ; the precise dependence is clarified later. More explicitly, one finds:

$$F(\phi, z) = \frac{1}{\sqrt{1-z^2}} \left[g F_g(\phi, z) - g_R N_{rl} \left(\frac{\gamma_c}{\gamma_R} \right) F_{g_R}(\phi, z) \right], \quad (17)$$

a nonlinear function of z with multi-harmonic ϕ -dependence. Note that the coupling term may also be divided into a g -mediated term $\propto F_g$ and a g_R -mediated term $\propto F_{g_R}$; the latter is again weaker in this regime by the factor γ_c/γ_R . The explicit forms of these functions may be found in appendix B. Most importantly, we find the coupling

term is approximately unchanged under $z \rightarrow -z$, which is very different from the behaviour of the detuning term.

Both detuning and coupling terms combine to determine the possibility of a synchronised phase via equation (13). This is best explored graphically; we first consider the g -mediated regime, where $g_R = 0$. In figure 2(b), we plot $\max_{\phi} / \min_{\phi} \{\rho F(\phi, z)\}$ (dashed black) and $\Omega(z, \rho)$ (solid blue) for fixed ρ , over the entire range of $z \in [-1, 1]$. The value of ρ is proportional to the pump power: the left panel is for $\rho = 10$, while the right panel shows $\rho = 40$, corresponding to an increased pump power. Equation (13) for $\dot{\phi} = 0$ is satisfied in the shaded regions; here the detuning term lies within the range of the coupling term as determined by the dashed curves. Hence, in the *unshaded* regions, synchronisation is impossible; clearly, the $z < 0$ region is preferred for synchronisation here, a result stemming from the reduced value of Ω for this configuration. With increasing pump power, the shaded region area grows, as the increasing coupling strength and detuning modification make synchronisation easier. The analogous plot in the g -mediated regime ($g = 0$) is shown in figure 2(c), for $\rho = 10$ and $\rho = 30$. Here, the situation is effectively reversed: the different mechanism for frequency modification means that the detuning term (solid red) is reduced for $z > 0$ instead, whereas the coupling term (dashed black) is mostly unchanged. As a result, synchronisation is preferred here for the $z > 0$ configuration.

4. Stability analysis and phase diagram

4.1. Stability maps

The intuitive description of the previous section places constraints on the $\dot{\phi} = 0$ state, but does not guarantee synchronisation; a complete analysis requires studying the full system of equations given by:

$$\dot{\phi} = 0 = \Delta\omega_0 - \rho G_{\phi}(\phi, z), \quad (18a)$$

$$\dot{z} = 0 = (\gamma_l - \gamma_r)(1 - z^2) + \rho G_z(\phi, z), \quad (18b)$$

$$\dot{\rho} = 0 = \rho[(\gamma_l + \gamma_r) + (\gamma_l - \gamma_r)z - \rho G_{\rho}(\phi, z)]. \quad (18c)$$

Here we have rewritten equation (12) to isolate the bare pump mode detuning, $\Delta\omega_0$. $G_{\phi, z, \rho}$ are functions of system parameters and the variables (ϕ, z) only. The explicit forms of these functions are provided in appendix B; we will find that the expressions above can already yield useful insight. While equations (18a)–(18c) cannot be analytically solved for the fixed points, progress can be made if both modal gains are taken to be equal, $\gamma_l(P) \approx \gamma_r(P)$. Recall that the $\gamma_n(P)$ are pre-determined by solving the non-Hermitian problem for the pump modes; we find the modal gains are indeed numerically equal in the present case. Note that this is also the most interesting scenario, since neither mode is preferred over the other by the pump.

We consider fixing all system parameters other than the pump power. The $\dot{\rho}$ equation can then be solved to obtain the parametric dependence (on ϕ and z) of the fixed points of ρ ,

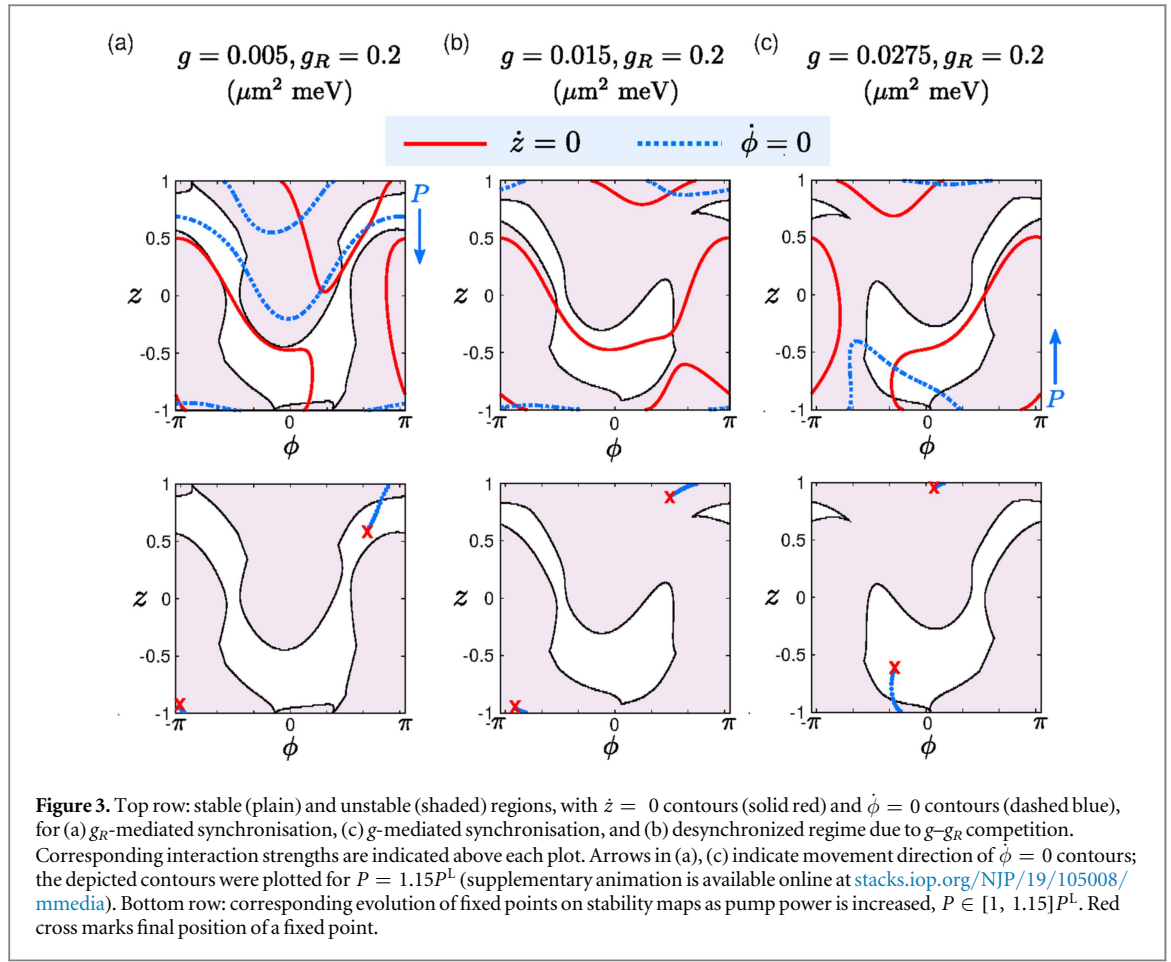
$$\rho_{\text{FP}} = \frac{\gamma_l(P) + \gamma_r(P)}{G_{\rho}(\phi, z)}. \quad (19)$$

The dominant power dependence here comes from the evolution of $\gamma_n(P)$, which is shown in figure 1(c). The function $G_{\rho}(\phi, z)$ in the denominator is independent of P , and hence for a given (ϕ, z) pair, the steady state value of ρ evolves *linearly* with pump power. In what follows, it is then justified to use ρ as a surrogate variable for the pump power P . The \dot{z} equation also simplifies to $\dot{z} = 0 = \rho G_z(\phi, z)$. This implies that the values of (ϕ, z) for which \dot{z} vanishes are unchanged with increasing ρ , and hence pump power.

In addition to the existence of fixed points in $\{\phi, z, \rho\}$ space, a persistent synchronised phase demands that such fixed points be dynamically stable. We find that a standard stability analysis of equations (18a)–(18c) based on the eigenvalues λ of the associated Jacobian matrix \mathbf{J} also benefits from the simplified ρ dependence. At the fixed points, we have:

$$\mathbf{J}(\phi, z, \rho)|_{\text{FP}} = \rho \begin{pmatrix} -\partial_{\phi} G_{\phi} & -\partial_z G_{\phi} & -\frac{\Delta\omega_0}{\rho^2} \\ \partial_{\phi} G_z & \partial_z G_z & 0 \\ -\rho \partial_{\phi} G_{\rho} & -\rho \partial_z G_{\rho} & -G_{\rho} \end{pmatrix} \Big|_{\text{FP}}. \quad (20)$$

The matrix element $\propto \Delta\omega_0 / \rho^2$ yields terms in the characteristic equation that are suppressed by $1/\rho$ relative to remaining contributions at the same order. For large enough ρ , this term may be dropped; then, the resulting Jacobian matrix has a characteristic equation $\chi(\phi, z, \lambda/\rho) = 0$, with a crucial implication: the ρ dependence of the characteristic equation serves only to scale its roots, the eigenvalues of \mathbf{J} . This result is explicitly derived in appendix D. Hence, the *sign* of any eigenvalue does not change as ρ , and therefore pump power, is changed. While this conclusion holds only approximately, and that too at the fixed points of equations (18a)–(18c) at any



pump power, we find that in practice the signs of eigenvalues of \mathbf{J} are quite robust to changes in ρ , for values of ρ close to ρ_{FP} at that pump power. Thus, for any fixed set of system parameters, stable regions where all eigenvalues of \mathbf{J} have negative real parts, and unstable regions where at least one eigenvalue has positive real part, are approximately *unchanged* with pump power. Because ϕ - z space is bounded in $[-\pi, \pi] \times [-1, 1]$, the emergence and movement of fixed points with increasing pump power can be tracked on finite, fixed *stability maps* of stable and unstable regions to characterise the global behaviour of the system (even though the entire space is not explored for any given initial condition).

An example of a stability map is shown for the g_R -mediated regime in figure 3(a), with plain regions being stable and shaded regions unstable, and the $\dot{z} = 0$ contours shown in solid red; all of these features are unchanged with pump power. Only the $\dot{\phi} = 0$ contours (dashed blue) change with P ; note that such a contour only exists at points where condition (13) is satisfied. Hence we can now see how the generalised Adler equation plays a defining role in the emergence of a synchronised phase with increasing pump power. In the g_R -mediated regime, it is clear from figure 2(c) that the $\dot{\phi} = 0$ contours prefer the $z > 0$ region. The trajectories of fixed points with P are shown in the lower panel of figure 3(a). The fixed point in the $z > 0$ region flows with increasing P and enters the stable region; as this crossing occurs, a synchronised phase of the system becomes stable. Note that in the $z < 0$ region, the $\dot{z} = 0$ contour exists in a stable region; however, a stable fixed point cannot emerge until the $\dot{\phi} = 0$ contour spreads in this region, which is clearly restricted based on our analysis of the generalised Adler equation (see figure 2(c)). In contrast, figure 3(c) shows a stability map in the g -mediated regime. Here, the $\dot{\phi} = 0$ contours prefer instead the $z < 0$ region, again clear from figure 2(b). As such, the fixed point that flows from an unstable to a stable region now has $z < 0$.

Most interestingly, an intermediate regime exists where the two interactions compete; the different scaling of detuning and coupling terms discussed earlier implies that for this regime, $g \sim g_R(\gamma_c/\gamma_R)$. A typical stability map here is shown in figure 3(b). For the same range of pump strengths as figures 3(a) and (c), the $\dot{\phi} = 0$ contours barely move; this is due simply to the competing effects of g - and g_R -mediated frequency modification. As a result, while there are stable regions where $\dot{z} = 0$ contours also exist, these are not accessible to the almost static $\dot{\phi} = 0$ contours. Hence, no stable fixed point emerges and a desynchronized phase persists (supplementary animation showing the movement of $\dot{\phi} = 0$ contours in figure 3 can be found online).

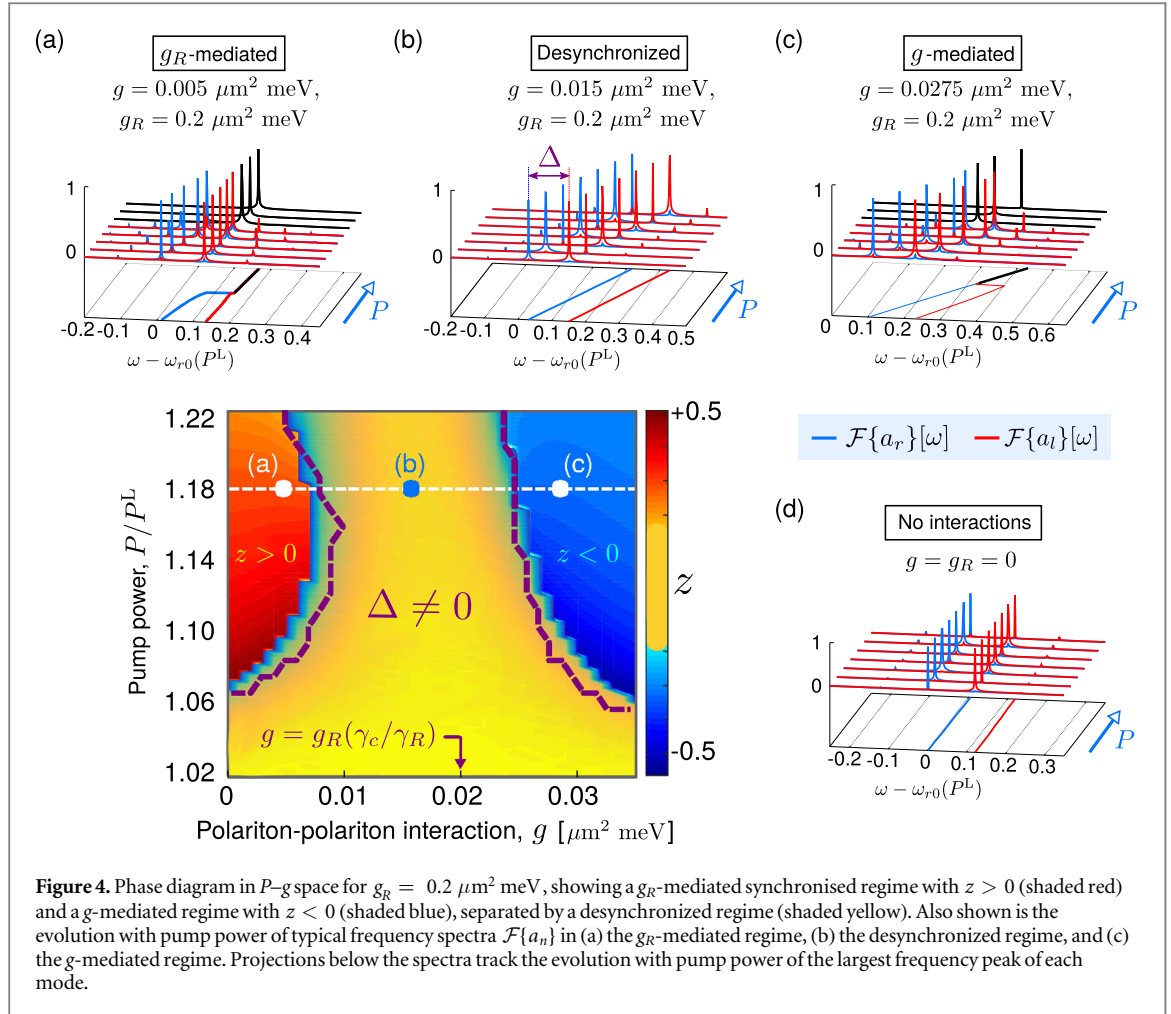
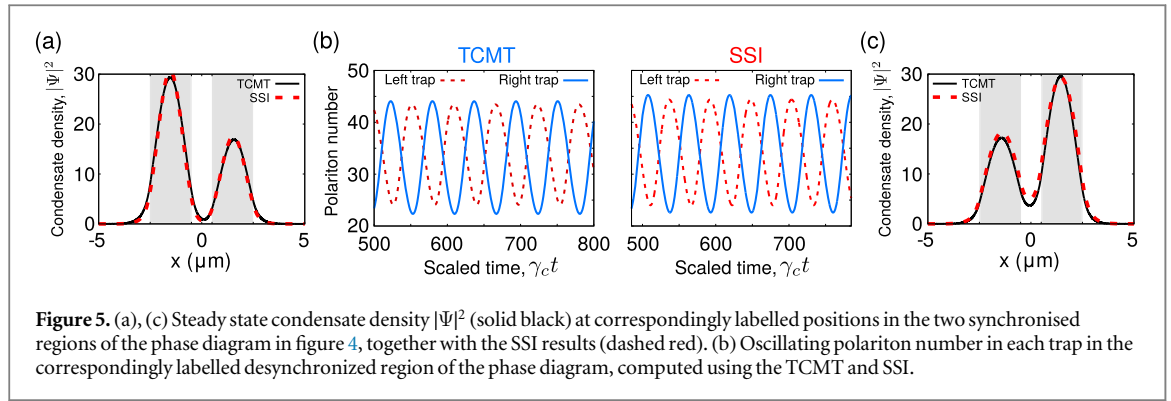


Figure 4. Phase diagram in P - g space for $g_R = 0.2 \mu\text{m}^2 \text{ meV}$, showing a g_R -mediated synchronised regime with $z > 0$ (shaded red) and a g -mediated regime with $z < 0$ (shaded blue), separated by a desynchronised regime (shaded yellow). Also shown is the evolution with pump power of typical frequency spectra $\mathcal{F}\{a_n\}$ in (a) the g_R -mediated regime, (b) the desynchronised regime, and (c) the g -mediated regime. Projections below the spectra track the evolution with pump power of the largest frequency peak of each mode.

4.2. Phase diagram

The predictions of the previous sections manifest strikingly in a phase diagram obtained via full numerical integration of the TCMT. We simulate the dynamical mode coefficients $a_n(t)$ to long times until a steady state is reached, and then compute the modal detuning Δ from the Fourier transform of mode coefficients, $\mathcal{F}\{a_n\}$. This procedure is repeated for varying pump strengths P and increasing values of the polariton-polariton interaction strength g , starting from $g = 0$; importantly, the reservoir-polariton interaction strength is kept fixed at $g_R = 0.2 \mu\text{m}^2 \text{ meV}$. A plot of the computed detuning Δ in P - g space constitutes the phase diagram shown in figure 4. In the yellow shaded regions, a desynchronised solution persists ($\Delta \neq 0$). Outside this region, the modal detuning vanishes and the two modes synchronise. Clearly, three distinct dynamical regimes can be identified, which we will now describe. For weak enough values of $g \ll g_R(\gamma_c/\gamma_R)$, a synchronised state emerges beyond a threshold pump power. In this region, the typical pump dependence of the Fourier spectra $\mathcal{F}\{a_n\}$ of mode coefficients is shown in figure 4(a). The curves projected below the spectra depict the evolution of the mode frequencies as a function of pump power. Clearly, the modes experience a frequency blueshift due to interactions as the pump is increased (dotted lines indicate constant frequency). This continues until the threshold power is reached, beyond which a single frequency synchronised state emerges (indicated in solid black). In the synchronised case, $\dot{\phi} = \dot{z} = \dot{\rho} = 0$ in the steady state; we thus superimpose the steady state population imbalance in this synchronised regime on figure 4. For weak g , the polariton configuration appears with $z > 0$ (shaded red), in what we label as the regime of g_R -mediated synchronisation.

With stronger $g \sim g_R(\gamma_c/\gamma_R)$, the predicted competition between the two types of frequency modulation effects does in fact arise, and the synchronised state disappears. Typical frequency spectra $\mathcal{F}\{a_n\}$ in this regime, shown in figure 4(b), still indicate a frequency blueshift due to interactions, but the modes remain detuned. In this interacting regime, dynamics are reminiscent of ac Josephson oscillations between the coupled condensates (see section 4.3). For values of g that are stronger still, a synchronised phase emerges once more, but now with $z < 0$ (shaded blue). In this g -mediated regime where interactions are strongest, the frequency blueshift is most pronounced, as is clear from the Fourier spectra in figure 4(c). Again, the blueshifted modes lock to a single frequency beyond a synchronisation power threshold.



The threshold for synchronisation in both the g_R -mediated and g -mediated regimes is predicted very well by our analysis of fixed points with $\dot{\phi} = \dot{z} = \dot{\rho} = 0$ moving on a fixed stability map. The stability map is computed at fixed $P = 1.15P^L$, making use of our previous result that stable and unstable regions are approximately unchanged with pump power. The phase boundary computed via this analysis is shown in dashed purple in figure 4. The slight discrepancy near the phase boundary may be explained as follows: for pump powers above the dashed purple line, the synchronised solution becomes stable; however, in a narrow range of pump powers, the initial condition determines whether the system settles into the synchronised phase or remains desynchronised. We note that this bistability of synchronised and desynchronised solutions is similar to results found in another two-mode configuration by Borgh *et al* [47].

Interestingly, for the pump range studied here, a synchronised state does not emerge if both interactions are turned off. For this case where $g = g_R = 0$, the Fourier spectra of mode coefficients as a function of pump power are shown in figure 4(d). The modes experience no blueshift, as expected, and the modal detuning is unchanged with pump power. Therefore, while the presence of either a dominant polariton–polariton interaction or reservoir–polariton interaction is *necessary* for synchronisation, the competition of *both* interactions actually hinders synchronisation.

Finally, one may note that the value of g_R used in figure 4 is strong relative to g ; this is chosen to make clear the role played by reservoir–polariton interactions in synchronisation. Phase diagrams for weaker g_R values are included in appendix E, figure E1. The g_R -mediated synchronisation region generally shrinks and can even disappear for weaker values of the reservoir–polariton interaction strength. However, the key element—the competing nature of the interactions—still remains: if for $g_R = 0$ and a fixed nonzero g , a g -mediated synchronised state emerges at a given pump strength, then nonzero g_R pushes up this pump strength, and for strong enough g_R may even lead to g_R -mediated synchronisation.

4.3. Comparisons with SSI

Since the TCMT is derived directly from the gGPE, a well-defined comparison between TCMT simulations of the previous section and a symplectic split-step integration (SSI) of the gGPE (see equations (1a) and (1b)) can be made. In the one-dimensional geometry under consideration, we find that the two-mode TCMT is between one to two orders of magnitude faster than the SSI at a given pump power, for an equivalent spatial resolution and final integration time. The efficiency is primarily due to the TCMT’s avoidance of spatial integration at every time step via a modal expansion. This fact also saves the TCMT’s computation times from an unfavourable scaling with spatial dimension. SSI computation times, on the other hand, scale exponentially with dimension d , as $N_g^d \log(N_g)$ for a spatial grid with (uniform) density N_g [48], which should render the TCMT even more favourable in higher dimensions (not considered here).

Thus, instead of computing the full phase diagram using the SSI, we provide select comparisons of TCMT and SSI results; in particular this is done for distinct points along the horizontal dashed white line in figure 4, which stretches across the three distinct dynamical regimes. In the synchronised regimes, at positions labelled (a) and (c) on the phase diagram, the condensate density is stationary in the steady state as mentioned earlier. We thus compare $|\Psi|^2$, shown in figures 5(a) and (c) respectively; TCMT results are in solid black, and SSI results in dashed red. Note that the synchronised configurations in (a) and (c) are distinct from self-trapped states in coupled condensates [35]. This is particularly clear in the ϕ – z plane: while frequency synchronisation leads to a constant relative phase (and population imbalance) as discussed earlier, the self-trapped regime has a relative phase that drifts linearly in time, and population imbalance that is weakly oscillating [49].

In the desynchronised regime, the mode amplitudes contain multiple frequencies unlike the synchronised case (see figure 4(b)). The condensate density is then no longer stationary in time. Here a plot of the polariton

occupations in each trap, in figure 5(b), indicates ac Josephson-like oscillations between the detuned traps, with a running phase [20, 35, 47, 50, 51]. The TCMT and SSI exhibit excellent agreement in all three cases, which helps validate the preceding results of the two-mode TCMT.

Lastly, the dynamics of the reservoir across the synchronised and desynchronised regimes may also be computed using both methods; these results are included in appendix E for completeness, and are also found to agree well.

5. Conclusions and outlook

In this paper we have investigated the synchronisation of two detuned, coupled polariton modes as a function of pump power, with a particular focus on the role played by the different nonlinear interactions unique to pumped polaritonic systems. Our analysis is based on a TCMT that allows both analytical insight and efficient numerical simulations. We find that the polariton configuration in the emergent synchronised phase is strongly dependent on the relative influence of polariton–polariton and reservoir–polariton interactions. Most interestingly, the two types of interactions can have competing effects that prevent the emergence of a synchronised phase altogether. This conclusion is verified against direct simulation of the generalised Gross–Pitaevskii equation and very good agreement is found.

A natural extension of this work is to larger coupled systems, such as polariton lattices [52]. In particular, in recently realised flat band condensation [36], polariton states are highly localised due to disorder, while still possessing a finite frequency dispersion. The original experiment was concerned with threshold physics under weak pumping, and thus the polariton–polariton nonlinearity played a negligible role. However under stronger pumping, the relative strengths of reservoir–polariton and polariton–polariton interactions could be crucial in determining whether or not a spatially extended, synchronised (single-frequency) condensate could be formed, and what spatial configuration such a condensate may take. For studies in modern polariton lattice structures, the work here can be extended to regimes where $\gamma_R \lesssim \gamma_c$; the regimes directly studied in this paper should still be relevant in disorder-generated polariton trap geometries [21, 34]. More generally, our results uncover an additional role of reservoir-mediated interactions in condensate dynamics, adding to other effects studied recently including the dynamical reservoir regime, multimode dynamics, and instabilities [33, 40, 41].

Acknowledgments

We thank F Marquardt for helpful discussions. This work was supported by the US Department of Energy, Office of Basic Energy Sciences, Division of Materials Sciences and Engineering under Award No. DE-SC0016011.

Appendix A. Additional details of TCMT derivation

To project equations (1a) and (1b) onto the non-Hermitian TCMT basis, it is useful to first rewrite equation (1a) under a displacement transformation of the reservoir density:

$$n_R(\mathbf{r}, t) = \tilde{n}_R(\mathbf{r}, t) + \frac{P}{\gamma_R} f(\mathbf{r}). \quad (\text{A.1})$$

Here, $\tilde{n}_R(\mathbf{r}, t)$ is the nonlinear, time-dependent part of the reservoir density that describes the depletion of the linear part. Under this transformation, and using the definition of $\mathcal{H}_L(P)$ in equation (2), the gGPE can be rewritten as:

$$i\partial_t \Psi = [\mathcal{H}_L(P) + s\gamma_R \tilde{n}_R(\mathbf{r}, t) + g|\Psi|^2] \Psi. \quad (\text{A.2})$$

This equation can then simply be projected onto the basis modes $\{\varphi_n\}$ using the expansion in equation (6) and the orthogonality relation (5). The resulting modal equations for the coefficients $a_n(t)$ then become equation (7a) of the main text.

The dynamical equation for the full reservoir density n_R , equation (1b), requires some more work. In particular, we employ the continuity equation for this non-Hermitian system, which has the form:

$$\vec{\nabla} \cdot \vec{j} + \partial_t |\Psi|^2 = R n_R |\Psi|^2 - \gamma_c |\Psi|^2, \quad (\text{A.3})$$

where \vec{j} is the polariton current,

$$\vec{j} = \frac{i}{2m}(\Psi \vec{\nabla} \Psi^* - \text{c.c.}). \quad (\text{A.4})$$

The left-hand side of (A.3) is familiar from the continuity equation for closed systems, while the right-hand side describes modifications due to the non-Hermitian nature of this driven-dissipative system. These include gain from the reservoir $\propto R$, and losses $\propto \gamma_c$. Here, we employ the continuity equation to rewrite the reservoir-condensate coupling term in equation (1b) in terms of condensate-only terms. The rewritten reservoir dynamics equation following this substitution and the displacement transformation of equation (A.1) takes the form:

$$\partial_t \tilde{n}_R = -\gamma_R \tilde{n}_R - \partial_t |\Psi|^2 - \gamma_c |\Psi|^2 - \vec{\nabla} \cdot \vec{j}. \quad (\text{A.5})$$

The above equation is now in a convenient form to be projected onto the non-Hermitian basis. Again employing the basis expansion in equation (6), then multiplying through by $\varphi_n \varphi_m$ and integrating over \mathcal{P} , we arrive at equation (7b) for the dynamical reservoir matrix elements.

Appendix B. Full equations for dynamical variables

We now present the full forms of the dynamical equations for variables $\{\phi, z, \rho\}$, obtained from equations (7a) and (7b) via the transformation defined in the main text, equation (10). In what follows, the overlap matrix elements A_{nmkq} , B_{nmkq} are as defined in equation (9), while the reservoir matrix elements are scaled to extract out the explicit dependence on ρ , $N_{nm} \rightarrow \rho \frac{\gamma_c}{\gamma_R} N_{nm}$.

We begin with the equation for the relative phase ϕ ,

$$\dot{\phi} = \Delta\omega_0 - \rho G_\phi(\phi, z). \quad (\text{B.1})$$

The bare detuning $\Delta\omega_0 = \omega_l(P) - \omega_r(P)$, as presented in the main text. The function $G_\phi(\phi, z)$ can be written as:

$$G_\phi(\phi, z) = -\frac{1}{2} \left[\left(\frac{\gamma_c}{\gamma_R} \right) N_\phi(\phi, z) + g K_\phi(\phi, z) \right]. \quad (\text{B.2})$$

Here, $N_\phi(\phi, z)$ contains the reservoir matrix elements:

$$N_\phi(\phi, z) = 2g_R(N_{ll} - N_{rr}) - \frac{1}{\sqrt{1-z^2}} N_{rl}(2R \sin \phi + 4zg_R \cos \phi). \quad (\text{B.3})$$

The function $K_\phi(\phi, z)$ describes polariton–polariton repulsion terms:

$$K_\phi(\phi, z) = \frac{\cos \phi}{\sqrt{1-z^2}} [(1-z^2)(A_{llr} + 2A_{lll} - A_{rrl} - 2A_{rrr}) - (1+z)^2 A_{rll} + (1-z)^2 A_{lrr}] \\ + \cos 2\phi [(1-z)A_{lrl} - (1+z)A_{rll}] + (1+z)(A_{lll} - 2A_{rll}) - (1-z)(A_{rrr} - 2A_{llr}). \quad (\text{B.4})$$

To compare with the form of the generalised Adler equation of section 3, the full expression for the detuning term $\Omega(z, \rho)$ contains simply the ϕ -independent terms from equation (B.1):

$$\Omega(z, \rho) = \Delta\omega_0 + g_R \rho \left(\frac{\gamma_c}{\gamma_R} \right) [N_{ll}(z) - N_{rr}(z)] \\ + \frac{1}{2} g \rho [(1+z)(A_{lll} - 2A_{rll}) - (1-z)(A_{rrr} - 2A_{llr})]. \quad (\text{B.5})$$

Note that $N_{nm}(z)$ is the ϕ -independent part of the reservoir matrix element N_{nm} . These parts will be made clear in due course. The coupling term of equation (17) contains all the ϕ -dependent terms from equation (B.1):

$$F(\phi, z) = \frac{1}{\sqrt{1-z^2}} \left[g F_g(\phi, z) - g_R N_{rl}(\phi, z) \frac{\gamma_c}{\gamma_R} F_{g_R}(\phi, z) \right]. \quad (\text{B.6})$$

Here, $N_{rl}(\phi, z)$ is the ϕ -dependent part of the matrix element N_{rl} . The functions F_g and F_{g_R} are defined as:

$$F_g(\phi, z) = \cos \phi [(1-z^2)(A_{llr} + 2A_{lll} - A_{rrl} - 2A_{rrr}) - (1+z)^2 A_{rll} + (1-z)^2 A_{lrr}] \\ + \cos 2\phi \sqrt{1-z^2} [(1-z)A_{lrl} - (1+z)A_{rll}] F_{g_R}(\phi, z) = \left(\frac{R}{g_R} \sin \phi + 2z \cos \phi \right). \quad (\text{B.7})$$

Next, we move on to the dynamical equation for the modal intensity imbalance, z , defined in the main text as:

$$\dot{z} = (\gamma_l - \gamma_r)(1 - z^2) - \rho G_z(\phi, z). \quad (\text{B.8})$$

Here, the function $G_z(\phi, z)$ has the form:

$$G_z(\phi, z) = -\frac{1}{2} \left[\left(\frac{\gamma_c}{\gamma_R} \right) N_z(\phi, z) + g K_z(\phi, z) \right]. \quad (\text{B.9})$$

As before, $N_z(\phi, z)$ contains the reservoir matrix elements:

$$N_z(\phi, z) = (1 - z^2)R(N_{ll} - N_{rr}) - \sqrt{1 - z^2}N_{rl}(2Rz \cos \phi - 4g_R \sin \phi) \quad (\text{B.10})$$

while the function $K_z(\phi, z)$ describes polariton–polariton repulsion terms:

$$\begin{aligned} K_z(\phi, z) = & \sin 2\phi [A_{rllr}(1 + z - z^2 - z^3) + A_{lrll}(1 - z - z^2 + z^3)] \\ & - \sqrt{1 - z^2} \sin \phi [(1 - z^2)(A_{rrll} - A_{llrr} - 2A_{rlrr} + 2A_{llrl}) - A_{rlll}(1 + z)^2 - A_{lrrr}(1 - z)^2]. \end{aligned} \quad (\text{B.11})$$

Lastly, we move on to the dynamical equation for ρ :

$$\dot{\rho} = \rho [(\gamma_l + \gamma_r) + (\gamma_l - \gamma_r)z - \rho G_\rho(\phi, z)]. \quad (\text{B.12})$$

Now, $G_\rho(\phi, z)$ is:

$$G_\rho(\phi, z) = -\frac{1}{2} \left[\left(\frac{\gamma_c}{\gamma_R} \right) N_\rho(\phi, z) + g K_\rho(\phi, z) \right], \quad (\text{B.13})$$

where

$$N_\rho(\phi, z) = R[(1 + z)N_{ll} + (1 - z)N_{rr} + 2\sqrt{1 - z^2}N_{rl} \cos \phi] \quad (\text{B.14})$$

and

$$\begin{aligned} K_\rho(\phi, z) = & \sin 2\phi(1 - z^2)(A_{lrll} - A_{rllr}) \\ & + \sqrt{1 - z^2} \sin \phi [(A_{rrll} + A_{lrrr})(1 - z) - (A_{rlll} + A_{llrr})(1 + z) - 2(1 - z)A_{rlrr} + 2(1 + z)A_{llrl}]. \end{aligned} \quad (\text{B.15})$$

In all of the above, note that the reservoir matrix elements N_{nm} themselves are dynamical quantities that can be expressed in terms of the variables (ϕ, z) . In the regime where $\gamma_R \gg \gamma_c$, which is the case we consider in the main text, the reservoir dynamics can be adiabatically eliminated. This behaviour is inherited by the scaled reservoir matrix elements, which are then also bound to the condensate evolution such that the equations for $\{\phi, z, \rho\}$ are sufficient to determine condensate dynamics. We write the reservoir matrix elements N_{nm} in terms of a ϕ -dependent part $N_{nm}(\phi, z)$ and a ϕ -independent part $N_{nm}(z)$, such that:

$$N_{nm} = N_{nm}(\phi, z) + N_{nm}(z). \quad (\text{B.16})$$

Then, for the diagonal reservoir matrix elements, we find:

$$\begin{aligned} N_{rr}(z) = & \left[\frac{1 - z}{2\gamma_c} (2A_{rrrr}\gamma_r - B_{rrrr}\gamma_c P_{\text{fr}}) + \frac{1 + z}{2\gamma_c} (2A_{rlll}\gamma_l - B_{rlll}\gamma_c P_{\text{fr}}) \right], \\ N_{rr}(\phi, z) = & \frac{\sqrt{1 - z^2}}{2\gamma_c} [-(\omega_l - \omega_r)(A_{rrll} + A_{rllr}) \sin \phi \\ & + [(\gamma_l + \gamma_r)(A_{rrll} + A_{rllr}) - \gamma_c P_{\text{fr}}(B_{rrll} + B_{rllr})] \cos \phi] \end{aligned} \quad (\text{B.17})$$

and:

$$\begin{aligned} N_{ll}(z) = & \left[\frac{1 + z}{2\gamma_c} (2A_{llll}\gamma_l - B_{llll}\gamma_c P_{\text{fr}}) + \frac{1 - z}{2\gamma_c} (2A_{llrr}\gamma_r - B_{llrr}\gamma_c P_{\text{fr}}) \right], \\ N_{ll}(\phi, z) = & \frac{\sqrt{1 - z^2}}{2\gamma_c} [-(\omega_l - \omega_r)(A_{llrl} + A_{llrr}) \sin \phi \\ & + [(\gamma_l + \gamma_r)(A_{llrl} + A_{llrr}) - \gamma_c P_{\text{fr}}(B_{llrl} + B_{llrr})] \cos \phi]. \end{aligned} \quad (\text{B.18})$$

Finally, the ‘off-diagonal’ or ‘coupling’ reservoir matrix element $N_{rl} = N_{lr}$ can be similarly expressed by defining:

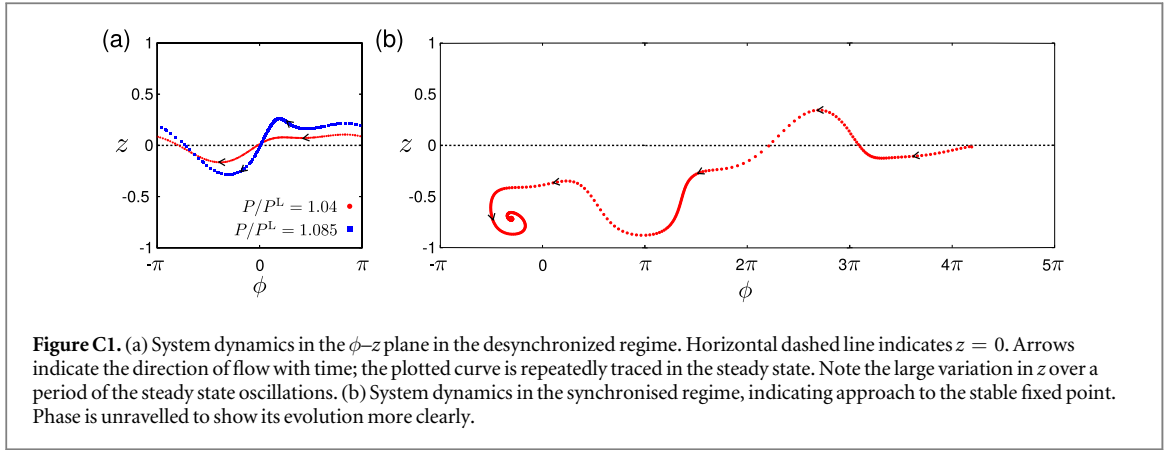


Figure C1. (a) System dynamics in the ϕ - z plane in the desynchronized regime. Horizontal dashed line indicates $z = 0$. Arrows indicate the direction of flow with time; the plotted curve is repeatedly traced in the steady state. Note the large variation in z over a period of the steady state oscillations. (b) System dynamics in the synchronised regime, indicating approach to the stable fixed point. Phase is unravelled to show its evolution more clearly.

$$N_{rl}(z) = \left[\frac{1-z}{2\gamma_c} (2A_{rlrr}\gamma_r - B_{rlrr}\gamma_c P_{fr}) + \frac{1+z}{2\gamma_c} (2A_{rllr}\gamma_l - B_{rllr}\gamma_c P_{fr}) \right],$$

$$N_{rl}(\phi, z) = \frac{\sqrt{1-z^2}}{2\gamma_c} [-(\omega_l - \omega_r)(A_{rlrl} + A_{rllr}) \sin \phi + [(\gamma_l + \gamma_r)(A_{rlrl} + A_{rllr}) - \gamma_c P_{fr}(B_{rlrl} + B_{rllr})] \cos \phi]. \quad (\text{B.19})$$

In all the above expressions, we have defined $P = P_{fr}P_0$, where $P_0 = \gamma_c \gamma_R / R$. Note that this ‘off-diagonal’ matrix element is proportional to the modal coupling at lowest order, while the ‘diagonal’ matrix elements do in fact contain a contribution that is independent of the modal coupling.

Appendix C. Phase space system dynamics

In this section we briefly discuss system dynamics for condensates in the coupled-trap geometry, as observed in the ϕ - z plane, in both the desynchronized and synchronised regimes. We start with initial conditions corresponding to very small initial modal occupations. The transient dynamics therefore involve a growing condensate density due to pumping, before a steady state is eventually reached. In the desynchronized regime, steady state curves are traced out in ϕ - z space, with examples shown in figure C1(a) in a typical case. Clearly, the large variation in z over a period indicates the complicated amplitude dynamics can not be assumed to be approximately static. Furthermore, with increasing pump power, larger amplitude oscillations for z are observed.

In the regime where a synchronised phase is possible, a stable fixed point exists as determined by the stability analysis described in the main text. Here, the system dynamically flows towards this fixed point in ϕ - z space. In the long time limit, the system localises at this fixed point; this is shown for a typical case in figure C1(b). We show results here by unwrapping the phase ϕ , for clarity. The exact details of the flow at a fixed pump power depend on initial conditions, as expected.

Appendix D. Jacobian matrix and stability

In this section we show that the Jacobian matrix corresponding to the system of equations for $\{\dot{\phi}, \dot{z}, \dot{\rho}\}$ (see equations (18a)–(18c)) takes on a particularly simple form in the regime of consideration. The equations are reproduced below, with the approximation $\gamma_l(P) \approx \gamma_r(P)$:

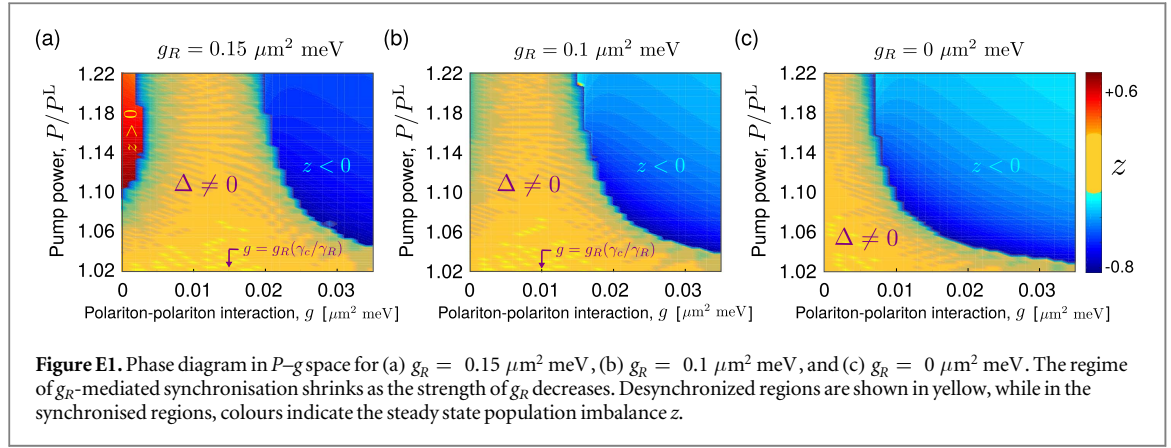
$$\dot{\phi} = 0 = \Delta\omega_0 - \rho G_\phi(\phi, z), \quad (\text{D.1a})$$

$$\dot{z} = 0 = \rho G_z(\phi, z), \quad (\text{D.1b})$$

$$\dot{\rho} = 0 = \rho [(\gamma_l + \gamma_r) - G_\rho(\phi, z)\rho]. \quad (\text{D.1c})$$

The associated Jacobian matrix for arbitrary (ϕ, z, ρ) is given by:

$$J(\phi, z, \rho) = \begin{pmatrix} -\rho \partial_\phi G_\phi & -\rho \partial_z G_\phi & -G_\phi \\ \rho \partial_\phi G_z & \rho \partial_z G_z & G_z \\ -\rho^2 \partial_\phi G_\rho & -\rho^2 \partial_z G_\rho & (\gamma_l + \gamma_r) - 2\rho G_\rho \end{pmatrix}. \quad (\text{D.2})$$



At any fixed point of the entire system of equations (D.1a)–(D.1c), the following constraints hold:

$$G_\phi = \frac{\Delta\omega_0}{\rho}, \quad G_z = 0, \quad G_\rho = \frac{\gamma_l + \gamma_r}{\rho} \implies (\gamma_l + \gamma_r) = \rho G_\rho. \quad (\text{D.3})$$

With these constraints, the Jacobian matrix simplifies to equation (20) of the main text,

$$\mathbf{J}(\phi, z, \rho)|_{\text{FP}} = \rho \begin{pmatrix} -\partial_\phi G_\phi & -\partial_z G_\phi & -\frac{\Delta\omega_0}{\rho^2} \\ \partial_\phi G_z & \partial_z G_z & 0 \\ -\rho\partial_\phi G_\rho & -\rho\partial_z G_\rho & -G_\rho \end{pmatrix} \Big|_{\text{FP}}. \quad (\text{D.4})$$

If we neglect the term $-\Delta\omega_0/\rho^2$, as justified in the main text, the characteristic equation $\chi = 0$ for this Jacobian matrix can be easily computed:

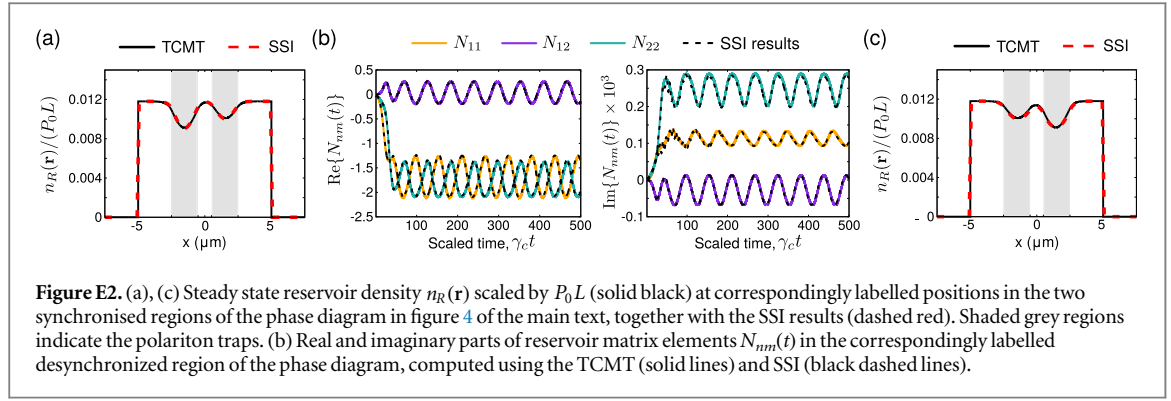
$$\begin{aligned} \det \mathbf{J} = 0 &= \rho^3 \left(-G_\rho - \frac{\lambda}{\rho} \right) \begin{bmatrix} -\partial_\phi G_\phi - \frac{\lambda}{\rho} & -\partial_z G_\phi \\ \partial_\phi G_z & \partial_z G_z - \frac{\lambda}{\rho} \end{bmatrix} \\ &= \rho^3 \left(-G_\rho - \frac{\lambda}{\rho} \right) \left[\left(-\partial_\phi G_\phi - \frac{\lambda}{\rho} \right) \left(\partial_z G_z - \frac{\lambda}{\rho} \right) + (\partial_\phi G_z)(\partial_z G_\phi) \right] \\ &= -\lambda^3 - \lambda^2 \rho (G_\rho + \partial_\phi G_\phi - \partial_z G_z) + \rho^3 G_\rho (\partial_\phi G_\phi)(\partial_z G_z) \\ &\quad - \lambda \rho^2 [G_\rho \partial_\phi G_\phi - G_\rho \partial_z G_z + (\partial_\phi G_z)(\partial_z G_\phi) - (\partial_\phi G_\phi)(\partial_z G_z)] \\ &= -\left(\frac{\lambda}{\rho} \right)^3 - \left(\frac{\lambda}{\rho} \right)^2 (G_\rho + \partial_\phi G_\phi - \partial_z G_z) + G_\rho (\partial_\phi G_\phi)(\partial_z G_z) \\ &\quad - \left(\frac{\lambda}{\rho} \right) [G_\rho \partial_\phi G_\phi - G_\rho \partial_z G_z + (\partial_\phi G_z)(\partial_z G_\phi) - (\partial_\phi G_\phi)(\partial_z G_z)], \\ \det \mathbf{J} = 0 &\equiv \chi(\phi, z, \lambda/\rho). \end{aligned} \quad (\text{D.5})$$

In the above, we require $\rho \neq 0$, which is the physically relevant case. The final result is referenced in the main text: the characteristic equation depends on ρ only via a scaling of the eigenvalues λ . As such, an increase in pump power does not change the sign of the eigenvalues, which is critical to determining stability.

Appendix E. Supplementary simulations and reservoir dynamics

In this section, we include additional simulation results to supplement those included in the main text. We begin by presenting phase diagrams in P - g space for values of g_R weaker than the value used for figure 4 of the main text. In figures E1(a)–(c), phase diagrams are plotted for $g_R = (0.15, 0.1, 0) \mu\text{m}^2 \text{ meV}$ respectively. Clearly, the g_R mediated synchronised regime shrinks as g_R becomes weaker. Note, however, that the reservoir-polariton interaction g_R still competes with synchronisation mediated by the polariton-polariton interaction strength g ; when g_R is turned off, the g -mediated synchronisation region is larger, over the same range of values of g , than the situation when $g_R \neq 0$.

In the main text we presented condensate dynamics; here, we briefly discuss the associated reservoir dynamics. In the synchronised regimes, corresponding to positions (a) and (c) in figure 4, the condensate has a single frequency. Both the condensate and reservoir densities become stationary in the long time limit; the latter



is then obtained by solving for the steady state of equation (1b):

$$n_R(\mathbf{r}) = \frac{Pf(\mathbf{r})}{\gamma_R + R|\Psi(\mathbf{r})|^2}. \quad (\text{E.1})$$

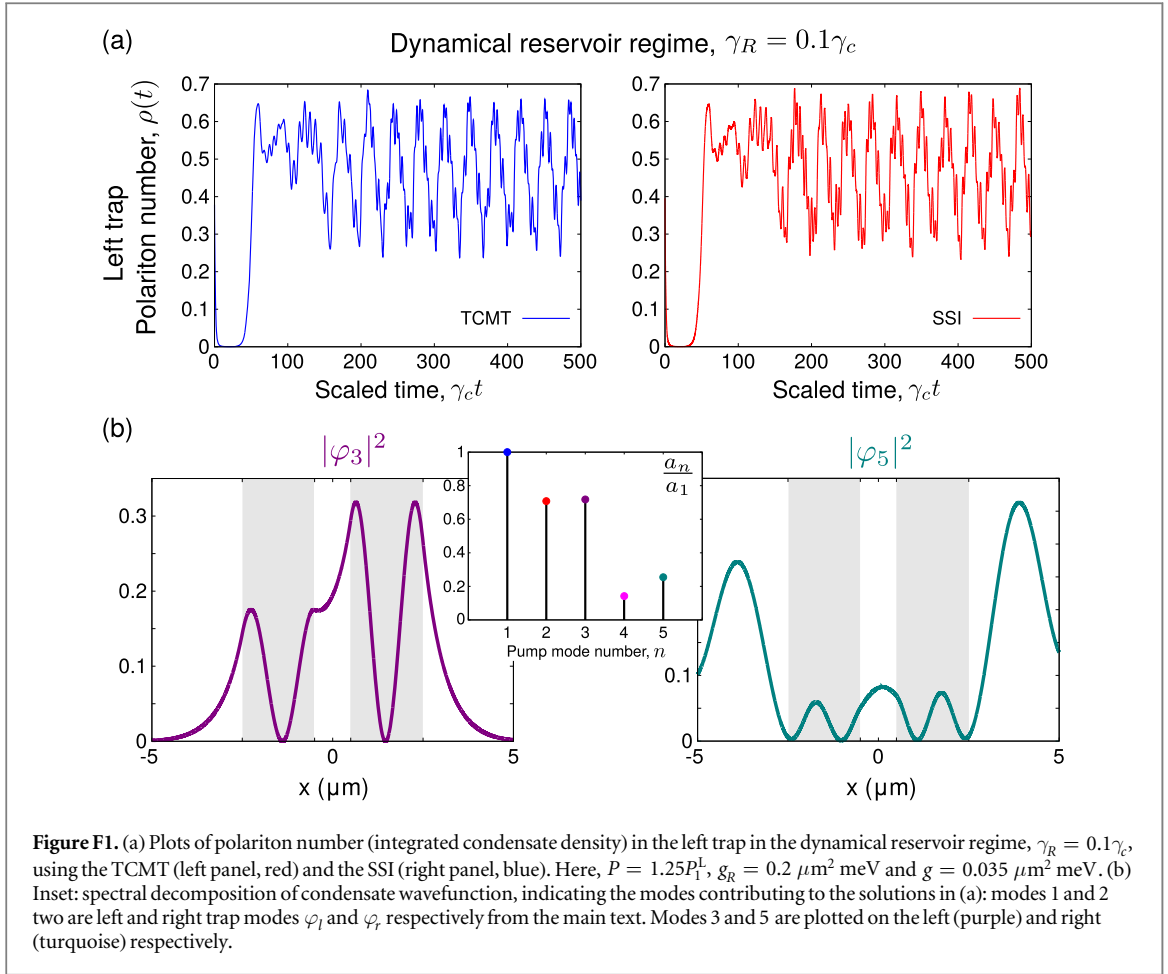
Recall that in our modal description of condensate dynamics, the TCMT can be used to obtain $|\Psi|^2$ but generally not the full reservoir density; instead, the simulated reservoir variables are the matrix elements $N_{nm}(t)$ (see equation (7b)). However, in the single frequency steady-state case, $n_R(\mathbf{r})$ is entirely determined by the condensate density, as is clear from equation (E.1). Thus the TCMT can be used to obtain $n_R(\mathbf{r})$ directly in this situation. We obtain the reservoir density, scaled by $P_0 L$, where L is the extent of the pump, and $P_0 = \gamma_c \gamma_R / R$ as introduced earlier, for positions (a) and (c) of figure 4. The results are shown in solid black in figures E2(a) and (c) respectively, and corresponding SSI results are shown in dashed red; note the excellent agreement. For (a), the synchronised phase has $z > 0$, and so the higher frequency, left trap mode has higher occupation. This indicates the condensate density is higher in the left trap, and thus the reservoir must be more strongly depleted there. This is precisely what is observed. For (c), where $z < 0$ instead, the reservoir overlapping with the right trap is more depleted, which agrees well with the simulated results.

In the desynchronized regimes, the reservoir density has a time-dependent evolution. In this more general case, a comparison of reservoir dynamics simulated by the TCMT and SSI can be carried out via the reservoir matrix elements instead. Using the full reservoir density computed via the SSI, $N_{nm}(t)$ may be obtained using the basis modes and equation (7b). Comparisons of the real and imaginary parts of the matrix elements are shown in figure E2(b) for the TCMT (solid lines) and SSI (dashed black). Again, excellent agreement is found.

Appendix F. Weak γ_R regime

The dynamics we consider in this paper, and the simplified stability analysis, hold for the case where $\gamma_R \gg \gamma_c$, namely the regime where the reservoir dynamics may be adiabatically eliminated. In the opposite, dynamical reservoir regime, where $\gamma_R \ll \gamma_c$, we have found that complex dynamical effects may arise, as found in recent numerical studies [33, 40]. In particular, strongly multimode behaviour emerges for high pumping powers and—more importantly for the physics considered here—for strong nonlinearities.

To illustrate further the kinds of multimode dynamics present in the dynamical reservoir regime, we present in figure F1(a) plots of the polariton number (integrated condensate density) in the left trap as a function of time using the TCMT, and an exact solution using an SSI, as in the main text, figure 4. Here, we take $\gamma_R = 0.1\gamma_c$; the remaining parameters are summarised in the figure caption. We find complex dynamical features that agree quite well between both methods. The emergence of these features is clarified via the modal description provided by the TCMT. In figure F1(b), the inset shows a spectral decomposition of the condensate wavefunction, plotting the normalised modal weights, $\frac{a_n}{a_1}$. Only peaks corresponding to the five modes with greatest spectral weight are shown; a total of eleven modes is needed to reach the agreement shown in figure F1(a). The first two modes are simply the left and right trap modes, φ_l and φ_r respectively. The two modes with next greatest spectral weight, modes number 3 and 5, are depicted in figure F1(b). Hence, in this regime where reservoir relaxation is slow relative to polariton loss, condensate dynamics can typically become very complicated, and may involve multiple interacting modes, as found here.



Appendix G. Neglecting exciton diffusion

The reservoir dynamical equation in equation (1a) typically includes an additional term incorporating the diffusion of excitons,

$$\partial_t n_R = Pf(\mathbf{r}) - \gamma_R n_R - R n_R |\Psi|^2 + \frac{D}{m} \nabla^2 n_R, \quad (\text{G.1})$$

where D is introduced as the *dimensionless* diffusion constant. In this paper, we have neglected this term, owing to this diffusion constant being relatively small for excitons due to their heavy mass; in typical systems [34] that we are considering here, $D \approx 10^{-3}$, which corresponds to actual diffusion rates on the order of 10 cm s^{-2} .

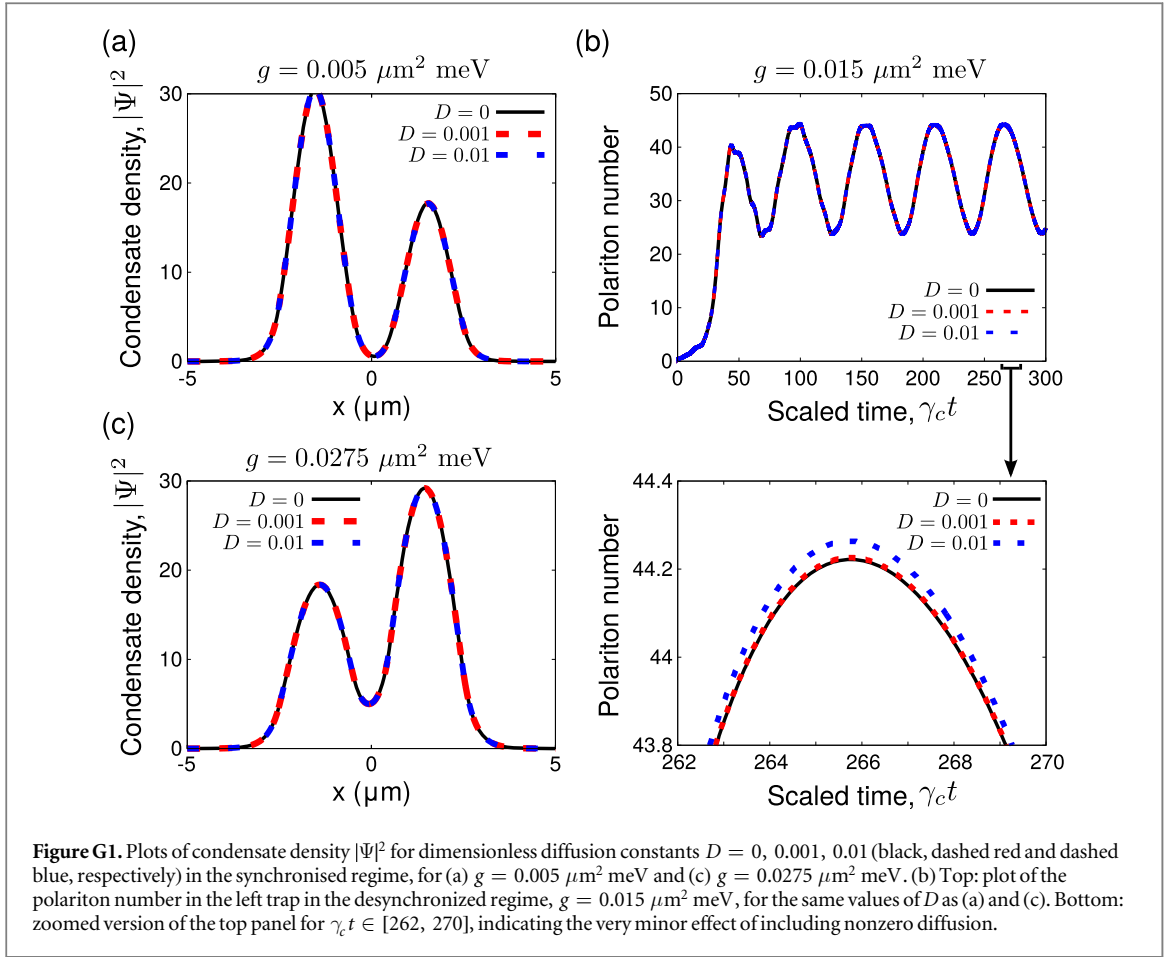
However, in the present case where reservoir depletion plays an important role in determining synchronisation dynamics, one may reasonably ask whether even relatively weak diffusion could strongly affect the observed physics. To verify that neglecting the diffusion term is valid, we first consider a perturbative solution in D ; the $D = 0$ reservoir dynamical equation can be solved when $\gamma_R \gg \gamma_c$, i.e. in the regime where the reservoir adiabatically follows the condensate evolution, to yield:

$$n_R^{(0)} = \frac{Pf(\mathbf{r})}{\gamma_R + R|\Psi^{(0)}|^2}. \quad (\text{G.2})$$

The superscript (0) indicates results computed with the diffusion term neglected ($D = 0$). If we now expand the full reservoir density for nonzero D as a power series in D , $n_R = n_R^{(0)} + D n_R^{(1)} + \dots$, a dynamical equation for the first order correction $n_R^{(1)}$ to first order in D is easily obtained:

$$\partial_t n_R^{(1)} = -\gamma_R n_R^{(1)} - R n_R^{(1)} |\Psi^{(0)}|^2 + \frac{1}{m} \nabla^2 n_R^{(0)}. \quad (\text{G.3})$$

In deriving the above, we have neglected the finite extent of the pump. Also, any modifications of $|\Psi|^2$ due to exciton diffusion will lead to contributions that are second order in D ; hence these are neglected. Again, in the regime of adiabatic elimination, the above equation may be solved:



$$n_R^{(1)} = \frac{1}{\gamma_R + R|\Psi^{(0)}|^2} \cdot \frac{1}{m} \frac{\partial^2}{\partial x^2} n_R^{(0)}. \quad (\text{G.4})$$

The effect of this correction to the diffusionless value $n_R^{(0)}$ can be estimated by computing the dimensionless ratio ν defined as:

$$\nu = \frac{\int d\mathbf{r} |\Psi^{(0)}|^2 D n_R^{(1)}}{\int d\mathbf{r} |\Psi^{(0)}|^2 n_R^{(0)}}. \quad (\text{G.5})$$

We compute the above quantity for a typical synchronised solution, and find $\nu \approx 0.01D$. This is a very small quantity, for which we expect almost no change with the inclusion of the diffusion term.

To further confirm the results of the above analysis, we perform SSI simulations of the gGPE while retaining the diffusion term in equation (G.1). We compute the numerical results for the three cases indicated in figures 4(a)–(c), and compare with the results for $D = 0$. The results are computed for $D = 10^{-3}$, and an order of magnitude stronger diffusion, $D = 10^{-2}$. The resulting plots are included in figures G1(a)–(c). We see a negligible difference between the $D = 0$ and $D \neq 0$ case; the bottom panel of figure G1(b) shows a zoomed in version of the desynchronised dynamics in the top panel, highlighting the minute discrepancy. The $D = 10^{-3}$ case is barely distinguishable from $D = 0$, while the use of a stronger diffusion constant also affects the dynamics only marginally. Certainly, no qualitatively different behaviour is observed. These simulations support the omission of the diffusion term in the reservoir dynamics for the systems considered here.

References

- [1] Kurths J, Pikovsky A and Rosenblum M 2001 *Synchronization: A Universal Concept in Nonlinear Sciences* (Cambridge: Cambridge University Press)
- [2] Matheny M H, Grau M, Villanueva L G, Karabalin R B, Cross M C and Roukes M L 2014 Phase synchronization of two anharmonic nanomechanical oscillators *Phys. Rev. Lett.* **112** 014101
- [3] Zhang M, Wiederhecker G S, Manapatruni S, Barnard A, McEuen P and Lipson M 2012 Synchronization of micromechanical oscillators using light *Phys. Rev. Lett.* **109** 233906
- [4] Holmes C A, Meaney C P and Milburn G J 2012 Synchronization of many nanomechanical resonators coupled via a common cavity field *Phys. Rev. E* **85** 066203

- [5] Bagheri M, Poot M, Fan L, Marquardt F and Tang H X 2013 Photonic cavity synchronization of nanomechanical oscillators *Phys. Rev. Lett.* **111** 213902
- [6] Wünsche H-J *et al* 2005 Synchronization of delay-coupled oscillators: a study of semiconductor lasers *Phys. Rev. Lett.* **94** 163901
- [7] Malik O, Makris K G and Türeci H E 2015 Spectral method for efficient computation of time-dependent phenomena in complex lasers *Phys. Rev. A* **92** 063829
- [8] Böhm F, Zakharova A, Schöll E and Lüdge K 2015 Amplitude-phase coupling drives chimera states in globally coupled laser networks *Phys. Rev. E* **91** 040901
- [9] Hush M R, Li W, Genway S, Lesanovsky I and Armour A D 2015 Spin correlations as a probe of quantum synchronization in trapped-ion phonon lasers *Phys. Rev. A* **91** 061401
- [10] Lee T E and Sadeghpour H R 2013 Quantum synchronization of quantum van der pol oscillators with trapped ions *Phys. Rev. Lett.* **111** 234101
- [11] Xu M, Tieri D A, Fine E C, Thompson J K and Holland M J 2014 Synchronization of two ensembles of atoms *Phys. Rev. Lett.* **113** 154101
- [12] Cawthorne A B, Barbara P, Shitov S V, Lobb C J, Wiesenfeld K and Zangwill A 1999 Synchronized oscillations in Josephson junction arrays: the role of distributed coupling *Phys. Rev. B* **60** 7575–8
- [13] Cross M C, Zumdieck A, Lifshitz R and Rogers J L 2004 Synchronization by nonlinear frequency pulling *Phys. Rev. Lett.* **93** 224101
- [14] Heinrich G, Ludwig M, Qian J, Kubala B and Marquardt F 2011 Collective dynamics in optomechanical arrays *Phys. Rev. Lett.* **107** 043603
- [15] Mari A, Farace A, Didier N, Giovannetti V and Fazio R 2013 Measures of quantum synchronization in continuous variable systems *Phys. Rev. Lett.* **111** 103605
- [16] Ludwig M and Marquardt F 2013 Quantum many-body dynamics in optomechanical arrays *Phys. Rev. Lett.* **111** 073603
- [17] Lee T E, Chan C-K and Wang S 2014 Entanglement tongue and quantum synchronization of disordered oscillators *Phys. Rev. E* **89** 022913
- [18] Lörch N, Amitai E, Nunnenkamp A and Bruder C 2016 Genuine quantum signatures in synchronization of anharmonic self-oscillators *Phys. Rev. Lett.* **117** 073601
- [19] Lörch N, Nigg S E, Nunnenkamp A, Tiwari R P and Bruder C 2017 Quantum synchronization blockade: energy quantization hinders synchronization of identical oscillators *Phys. Rev. Lett.* **118** 243602
- [20] Wouters M 2008 Synchronized and desynchronized phases of coupled nonequilibrium exciton–polariton condensates *Phys. Rev. B* **77** 121302
- [21] Baas A, Lagoudakis K G, Richard M, André R, Dang L S and Deveaud-Plédran B 2008 Synchronized and desynchronized phases of exciton–polariton condensates in the presence of disorder *Phys. Rev. Lett.* **100** 170401
- [22] Eastham P R 2008 Mode locking and mode competition in a nonequilibrium solid-state condensate *Phys. Rev. B* **78** 035319
- [23] Lugiato L A, Narducci L M and Oldano C 1988 Cooperative frequency locking and stationary spatial structures in lasers *J. Opt. Soc. Am. B* **5** 879
- [24] Tamm C 1988 Frequency locking of two transverse optical modes of a laser *Phys. Rev. A* **38** 5960–3
- [25] Tang D Y, Dykstra R and Heckenberg N R 1996 Synchronization of chaotic laser mode dynamics *Phys. Rev. A* **54** 5317–22
- [26] Ge L, Nersisyan A, Oztop B and Türeci H E 2013 Pattern formation and strong nonlinear interactions in exciton–polariton condensates (in preparation) (arXiv:1311.4847) [cond-mat, physics:nlm]
- [27] Galbiati M *et al* 2012 Polariton condensation in photonic molecules *Phys. Rev. Lett.* **108** 126403
- [28] Sun Y, Yoon Y, Khan S, Ge L, Pfeiffer L N, West K, Türeci H E, Snoko D W and Nelson K A 2016 Stable switching among high-order modes in polariton condensates (in preparation) (arXiv:1602.03024) [cond-mat, physics:quant-ph]
- [29] Marelic J, Zajiczek L F, Hesten H J, Leung K H, Ong E Y X, Mintert F and Nyman R A 2016 Spatiotemporal coherence of non-equilibrium multimode photon condensates *New J. Phys.* **18** 103012
- [30] Bennett M, Schatz M F, Rockwood H and Wiesenfeld K 2002 Huygens’s clocks *Proc. R. Soc. A* **458** 563–79
- [31] Huygens C 1673 *Horologium Oscillatorium* (Paris: Apud F. Muguet)
- [32] Türeci H E and Stone A D 2005 Mode competition and output power in regular and chaotic dielectric cavity lasers *Lasers and Applications in Science and Engineering (San Jose, CA, 2005)* **5708** 255
- [33] Khan S and Türeci H E 2016 Non-Hermitian coupled-mode theory for incoherently pumped exciton–polariton condensates *Phys. Rev. A* **94** 053856
- [34] Wouters M and Carusotto I 2007 Excitations in a nonequilibrium Bose–Einstein condensate of exciton polaritons *Phys. Rev. Lett.* **99** 140402
- [35] Abbarchi M *et al* 2013 Macroscopic quantum self-trapping and Josephson oscillations of exciton polaritons *Nat. Phys.* **9** 275–9
- [36] Baboux F *et al* 2016 Bosonic condensation and disorder-induced localization in a flat band *Phys. Rev. Lett.* **116** 066402
- [37] Wouters M, Carusotto I and Ciuti C 2008 Spatial and spectral shape of inhomogeneous nonequilibrium exciton–polariton condensates *Phys. Rev. B* **77** 115340
- [38] Türeci H E, Stone A D and Collier B 2006 Self-consistent multimode lasing theory for complex or random lasing media *Phys. Rev. A* **74** 043822
- [39] Ge L, Chong Y D and Stone A D 2010 Steady-state *ab initio* laser theory: generalizations and analytic results *Phys. Rev. A* **82** 063824
- [40] Bobrovska N, Ostrovskaya E A and Matuszewski M 2014 Stability and spatial coherence of nonresonantly pumped exciton–polariton condensates *Phys. Rev. B* **90** 205304
- [41] Bobrovska N and Matuszewski M 2015 Adiabatic approximation and fluctuations in exciton–polariton condensates *Phys. Rev. B* **92** 035311
- [42] Acebrón J A, Bonilla L L, Vicente C J P, Ritort F and Spigler R 2005 The Kuramoto model: a simple paradigm for synchronization phenomena *Rev. Mod. Phys.* **77** 137–85
- [43] Adler R 1946 A study of locking phenomena in oscillators *Proc. IRE* **34** 351–7
- [44] Razavi B 2004 A study of injection locking and pulling in oscillators *IEEE J. Solid-State Circuits* **39** 1415–24
- [45] Bhansali P and Roychowdhury J 2009 Gen-Adler: the generalized Adler’s equation for injection locking analysis in oscillators *2009 Asia and South Pacific Design Automation Conf.* pp 522–7 (<http://ieeexplore.ieee.org/document/4796533/>)
- [46] Mirzaei A and Darabi H 2014 Mutual pulling between two oscillators *IEEE J. Solid-State Circuits* **49** 360–72
- [47] Borgh M O, Keeling J and Berloff N G 2010 Spatial pattern formation and polarization dynamics of a nonequilibrium spinor polariton condensate *Phys. Rev. B* **81** 235302
- [48] Bader P, Blanes S and Casas F 2013 Solving the Schrödinger eigenvalue problem by the imaginary time propagation technique using splitting methods with complex coefficients *J. Chem. Phys.* **139** 124117

- [49] Albiez M, Gati R, Fölling J, Hunsmann S, Cristiani M and Oberthaler M K 2005 Direct observation of tunneling and nonlinear self-trapping in a single bosonic Josephson junction *Phys. Rev. Lett.* **95** 010402
- [50] Voronova N S, Elistratov A A and Lozovik Y E 2015 Detuning-controlled internal oscillations in an exciton–polariton condensate *Phys. Rev. Lett.* **115** 186402
- [51] Rahmani A and Laussy F P 2016 Polaritonic Rabi and Josephson oscillations *Sci. Rep.* **6** 28930
- [52] Milicevic M *et al* 2015 Edge states in polariton honeycomb lattices *2D Mater.* **2** 034012